

pHapCompass: Probabilistic Assembly and Uncertainty Quantification of Polyploid Haplotype Phase

Marjan Hosseini^{1,*}, Ella Veiner¹, Thomas Bergendahl¹, Tala Yassenpoor¹, Zane Smith², Margaret Staton²,
and Derek Aguiar^{1,3,*}

¹ School of Computing, University of Connecticut

² Department of Entomology and Plant Pathology, University of Tennessee

³ Institute for Systems Genomics, University of Connecticut

Abstract. Computing haplotypes from sequencing data, i.e. haplotype assembly, is an important component of foundational molecular and population genetics problems, including interpreting the effects of genetic variation on complex traits and reconstructing genealogical relationships. Assembling the haplotypes of polyploid genomes remains a significant challenge due to the exponential search space of haplotype phasings and read assignment ambiguity; the latter challenge is particularly difficult for polyploid haplotype assemblers since the information contained within the observed sequence reads is often insufficient for unambiguous haplotype assignment in polyploid genomes. We present pHAPCOMPASS, probabilistic haplotype assembly algorithms for diploid and polyploid genomes that explicitly model and propagate read assignment ambiguity to compute a distribution over polyploid haplotype phasings.

We develop graph theoretic algorithms to enable statistical inference and uncertainty quantification despite an exponential space of possible phasings. Since prior work evaluates polyploid haplotype assembly on synthetic genomes that do not reflect the realistic genomic complexity of polyploidy organisms, we develop a computational workflow for simulating genomes and DNA-seq for auto- and allopolyploids. Additionally, we generalize the vector error rate and minimum error correction evaluation criteria for partially phased haplotypes. Benchmarking of pHAPCOMPASS and several existing polyploid haplotype assemblers shows that pHAPCOMPASS yields competitive performance across varying genomic complexities and polyploid structures while retaining an accurate quantification of phase uncertainty. The source code for pHAPCOMPASS, simulation scripts, and datasets are freely available at <https://github.com/bayesomicslab/pHapCompass>.

Keywords: haplotype assembly, polyploidy, probabilistic graphical models

* To whom correspondence should be addressed. E-mail: marjan.hosseini@uconn.edu and derek.aguiar@uconn.edu

1 Introduction

Genomic variability is completely characterized by the sequences of genetic variant alleles along a single chromosome, or *haplotypes* [23]. Haplotypes are typically inferred computationally, since experimental determination of haplotypes requires specialized experimental protocols that are costly and challenging to implement [7]. Computational haplotyping is difficult since there exists 2^{n-1} possible haplotype explanations for a single diploid genotype with n heterozygous variants; the number of haplotype explanations grows even faster when the number of chromosome copies per cell is greater than 2 (i.e., for *polyploid* genomes) [3].

The two classes of algorithms for computing haplotypes are *haplotype phasing* and *haplotype assembly*. Haplotype phasing aims to compute haplotypes from multiple genotype sequences, which are determined using genotyping arrays [12] or DNA sequencing [14]. Haplotype phasing leverages haplotypes that are shared identical-by-descent within a population to phase the shared haplotype. However, haplotype phasing requires population data for diploid genomes and typically performs poorly for rare or *de novo* mutations [7,20]. In contrast, haplotype assembly leverages aligned and overlapping sequence reads to reconstruct haplotypes for a single diploid genome [33]. Haplotype assembly is well-defined for individual samples without a reference population and has been generalized for polyploid genomes [3].

Polyploid genomes add complexity to the haplotype assembly task in two significant ways. First, haplotypes of heterozygous single nucleotide polymorphisms (SNPs) are no longer complementary (Fig. 1). In diploid genomes with a known genotype, the resolution of one haplotype inherently produces the resolution of the complementary haplotype, such that the combination of the haplotypes is consistent with the genotype. In K -ploid genomes, $(K - 1)$ haplotypes must be resolved before leveraging genotype consistency to infer the final haplotype. Second, haplotype segments are not unique. Polyploid genomes can contain long segments (even chromosome length) of genetic material that is duplicated from the same (autopolyploidy) or similar (allopolyploidy) species. As a result, a single sequence read cannot be deterministically mapped to its chromosome of origin (e.g., the read in positions 0 and 1 in Fig. 1) and runs of homozygosity on any subset of haplotypes can result in a haplotype assembly fragmented into phased haplotype blocks (Fig. 1). In other words, uncertainty exists at multiple levels: both in terms of haplotype phase but also haplotype mapping uncertainty in the presence of identical haplotype segments. Statistical models provide a principled methodology for capturing polyploid phase uncertainty, but the exponential search space of polyploid haplotype phasings makes their formalization difficult. HapTree and Poly-Harsh are the only two existing statistical polyploid haplotype assemblers, but neither quantify haplotype phase uncertainty and considered only short-read sequencing [5,19].

In this work, we develop PHAPCOMPASS, a pair of statistical polyploid haplotype assembly models for long or short reads and benchmark PHAPCOMPASS on realistic autopolyploid and allopolyploid genomes. PHAPCOMPASS-short constructs a Markov random field where vertices denote discrete distributions over the haplotype phasings for a pair of SNPs and edges connect two haplotype phasings that share a SNP. Then, the PHAPCOMPASS-short inference algorithm leverages the pCompass graph, an exponentially-sized factor graph, to select subsets of SNP pairs to incorporate into the existing phasing. PHAPCOMPASS-long defines a chain graph (hybrid graphical model combining directed and undirected dependencies) that captures both the causal (directed) and mutual (undirected) dependencies. Explicit random variables encode both the haplotype sequences and the mapping of reads to haplotypes. Both algorithms allow for computing a single haplotype phasing using the Viterbi algorithm or quantifying phasing uncertainty using forward-filtering backward-sampling. We develop the first pipeline to simulate realistic autopolyploid or allopolyploid genomes and benchmark PHAPCOMPASS along with several leading polyploid haplotype assemblers with varied ploidy,

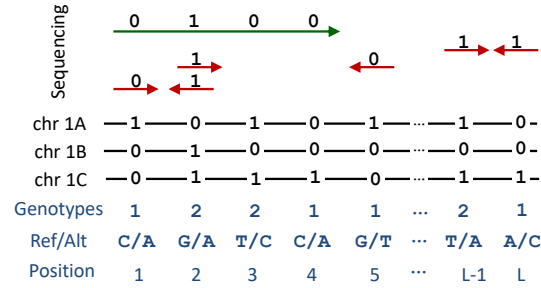


Fig. 1: **Haplotype assembly input for a triploid genome.** Long (green) or short (red) reads that cover two or more heterozygous SNPs (encoded as 0 or 1 for major or minor alleles) are informative of haplotype phase. A collection of overlapping reads (e.g., position 0-4) can be assembled into a single phasing (haplotype block) but their haplotype phase relative to other blocks is undetermined (e.g., positions $L - 1$ and L).

coverage, and mutation rates on both short and long read data. Lastly, we produce the first assembly of an allo-octoploid Strawberry chromosome. Source code, simulation scripts, and data are freely available at <https://github.com/bayesomicslab/pHapCompass>.

2 Related Work

Most haplotype assembly methods build a deterministic representation (typically a graph) whose complexity either scales with the number of sequence reads or genetic variants [33]. The first diploid human genome assembly was constructed using an algorithm that considers the assignment of reads to haplotypes by alternating two steps: (1) assign sequence reads to haplotypes and (2) compute haplotypes based on a majority vote of its assigned reads [24]. Although the Levy *et al.* algorithm is greedy, it was accurate and scaled well for the high quality and low throughput Sanger-based sequencing that was common in early genome assemblies. With the advent of short-read and high-throughput sequencing, methods began focusing on genetic variants instead of sequence reads. HapCut models genetic variants by defining a graph where vertices are heterozygous SNPs, edges connect two SNPs connected by at least one sequence fragment, and edge weights are proportional to the number of fragments that are inconsistent with a current phasing [4]. An iterative algorithm improves the haplotype assembly through maximum graph cuts; the successor algorithm HapCut2 extends HapCut by introducing a more sophisticated error model and support for different sequencing technologies [13]. In contrast, HapCompass [2], optimizes over the cycles of a graph where sequence reads (edges) provide evidence for the two phasings that can exist between two heterozygous SNP positions (vertices).

Extensions to polyploid genomes had to manage the uncertainty associated with multiple distinct haplotypes sharing the same or similar sequences and the non-complementarity of haplotypes in a phasing. The first polyploid haplotype assembly algorithm leveraged the HapCompass model [3], but the loss of the complement haplotype and haplotype uniqueness constraints made their cycle optimization approach scale poorly with the ploidy. The first statistical model for polyploid haplotype assembly, HapTree, searches for a maximum likelihood solution by growing polyploid assemblies one SNP in each iteration [5], whose probabilistic priors were extended in HapTree-X [6]. Another statistical assembler, Poly-Harsh, alternately samples haplotypes and read assignments [19], though neither method quantifies phasing uncertainty.

Inspired by the increasing lengths of PacBio and nanopore sequencing, more recent *long-read assembly* methods have shown improvements over HapCompass and HapTree-X by returning to model sequence reads as graph nodes. Sharing some similarities with HapCompass, Ranbow resolves conflicting cycles and paths in a multipartite graph [29]. Other methods such as SDhap [11], H-PoP and H-PoPG [37], nPhase [1], and WhatsHap [32] formalize polyploid assembly using generalized graph cuts or sequence read partitioning. Most recently, deep learning-based approaches are able to produce single haplotype block assemblies by leveraging correlations between non-overlapping reads, although the interpretation of this phenomenon is unclear [9,26]. In contrast to prior work, PHAPCOMPASS is the first diploid and polyploid assembler that quantifies uncertainty in haplotype assemblies; PHAPCOMPASS also benefits from two distinct statistical models designed to scale well with high coverage short reads (PHAPCOMPASS-short) or low coverage long reads (PHAPCOMPASS-long).

3 Methods

The haplotype assembly problem aims to reconstruct the haplotypes $H = \{h_1, \dots, h_K\}$ of an organism given a set of aligned sequencing reads $\mathcal{R} = \{r_j\}_{j=1}^{|\mathcal{R}|}$ spanning single nucleotide polymorphism (SNP) positions $\{1, \dots, L\}$ indexed by ℓ , a ploidy K , and genotype information $\mathcal{G} = \{g_1, \dots, g_L\}$ where $g_\ell \in \{1, \dots, K-1\}$. Sequence reads are informative of haplotype phase only if they cover at least two SNP positions (Fig. 1). For simplicity, we assume the SNPs are biallelic, i.e., each position has two possible alleles 0 and 1 denoting the reference and alternate allele, respectively. The reconstructed haplotypes are defined as $H^* = \{h_1^*, \dots, h_K^*\}$ where $h_k^* \in \{0, 1\}^L$. The haplotypes must satisfy the genotype constraint: $\sum_{k=1}^K h_k^*(\ell) = g_\ell \quad \forall \ell \in \{1, \dots, L\}$.

3.1 PHAPCOMPASS-short

Graph formalization and introducing the pCompass graph. The pCompass graph is the foundational data structure for the PHAPCOMPASS-short algorithm and is constructed from two related graphs. Let $\{\ell_0, \ell_1, \dots\}$ denote arbitrary SNP indices.

SNP Graph. The SNP graph $G = (V, E)$ represents the read overlaps where $V = \{1, \dots, L\}$ and an edge $(\ell_0, \ell_1) \in E$ if at least one read covers both SNP positions ℓ_0 and ℓ_1 (Fig. 2, Left). A read r “covers” SNP ℓ if the read overlaps with the position of SNP ℓ and the called base is 0 or 1; an uncovered SNP is denoted by ‘-’ [33].

SNP Line Graph. The SNP line graph $Q = (U, E_Q)$ is the line graph of G . Formally, each node $u_{\ell_0 \ell_1} \in U$ corresponds to an edge $(\ell_0, \ell_1) \in E$ of the SNP graph and two nodes in Q are adjacent if they share exactly one SNP position (Fig. 2, Middle). Formally,

$$E_Q = \{((\ell_0, \ell_1), (\ell_2, \ell_3)) : |\{\ell_0, \ell_1\} \cap \{\ell_2, \ell_3\}| = 1\}.$$

pCompass Graph. The pCompass graph is a factor graph constructed from Q that assigns potentials to all (not necessarily maximal) cliques based on observed read evidence (Fig. 2, Right). These potentials quantify the likelihood of different phasings given the sequencing data. The number of factors in the pCompass graph is exponentially sized with respect to $|U| = O(L^2)$, thus we only enumerate the 1- and 2-cliques of the graph. For each node $u_{\ell_0 \ell_1} \in U$, we define a *node potential* to be a function mapping elements in the space of valid phasings $\Phi_{\ell_0 \ell_1} \subset \{0, 1\}^{K \times 2}$ to \mathbb{R}_+ , where each phasing $\phi_{\ell_0 \ell_1}$ satisfies the genotype constraints:

$$\sum_{k=1}^K \phi_{\ell_0 \ell_1}^{(k)}(\ell_0) = g_{\ell_0} \quad \text{and} \quad \sum_{k=1}^K \phi_{\ell_0 \ell_1}^{(k)}(\ell_1) = g_{\ell_1},$$

where $\phi_{\ell_0 \ell_1}^{(k)} \in \{0, 1\}^2$ is the phasing for the pair of positions for haplotype k and $\phi_{\ell_0 \ell_1}^{(k)}(\ell_0)$ is the allele at position ℓ_0 . By parameterizing the space of valid phasings by $t_{11} = |\{k : \phi_{\ell_0 \ell_1}^{(k)} = (1, 1)\}|$, the count of haplotypes in the phasing with allele pattern (1, 1), we can enumerate all $|\Phi_{\ell_0 \ell_1}| = O(K)$ distinct phasings efficiently (see Appendix B). For each phasing $\phi_{\ell_0 \ell_1} \in \Phi_{\ell_0 \ell_1}$, we compute its node potential as:

$$f(\phi_{\ell_0 \ell_1}) = \sum_{r \in \mathcal{R}_{\ell_0 \ell_1}} \mathcal{L}(r, \phi_{\ell_0 \ell_1}), \quad \mathcal{L}(r, \phi_{\ell_0 \ell_1}) = \sum_{k=1}^K \varepsilon^{d(\phi_{\ell_0 \ell_1}^{(k)}, r[\ell_0, \ell_1])} (1 - \varepsilon)^{2 - d(\phi_{\ell_0 \ell_1}^{(k)}, r[\ell_0, \ell_1])},$$

where $\mathcal{R}_{\ell_0 \ell_1} = \{r \in \mathcal{R} : r[\ell_0] \neq '-' \wedge r[\ell_1] \neq '-'\}$ is the set of reads covering both positions, and $r[\ell_0, \ell_1]$ denotes the observed alleles in read r at these positions, $d(\cdot, \cdot)$ is the Hamming distance, and ε is the sequencing error rate. For each edge $e \in E_Q$ whose endpoints together cover three SNPs ℓ_0, ℓ_1, ℓ_2 , we define the *edge potential* over phasings of the three SNPs $\phi_{\ell_0 \ell_1 \ell_2} \in \Phi_{\ell_0 \ell_1 \ell_2} \subset \{0, 1\}^{K \times 3}$:

$$f(\phi_{\ell_0 \ell_1 \ell_2}) = \sum_{r \in \mathcal{R}_{\ell_0 \ell_1 \ell_2}} \mathcal{L}(r, \phi_{\ell_0 \ell_1 \ell_2}),$$

where $\mathcal{R}_{\ell_0 \ell_1 \ell_2} = \{r \in \mathcal{R} : r[\ell_0] \neq '-' \wedge r[\ell_1] \neq '-' \wedge r[\ell_2] \neq '-'\}$ is the set of reads covering all three positions, and

$$\mathcal{L}(r, \phi_{\ell_0 \ell_1 \ell_2}) = \sum_{k=1}^K \varepsilon^{d(\phi_{\ell_0 \ell_1 \ell_2}^{(k)}, r[\ell_0, \ell_1, \ell_2])} (1 - \varepsilon)^{3 - d(\phi_{\ell_0 \ell_1 \ell_2}^{(k)}, r[\ell_0, \ell_1, \ell_2])}.$$

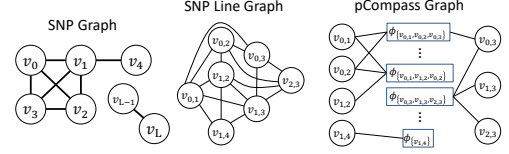


Fig. 2: **Graph constructions for pHapCompass-short inference.** *Left:* The SNP graph $G = (V, E)$ where vertices v_0, \dots, v_L represent heterozygous SNP positions and edges connect positions covered by at least one sequencing read. *Middle:* The SNP line graph $Q = (U, E_Q)$, where each node $v_{i,j}$ corresponds to an edge (i, j) in G , and two nodes are adjacent if their corresponding edges share exactly one SNP position. *Right:* The pCompass graph, a factor graph over Q where node potentials $\phi_{v_{i,j}}$ encode the likelihood of phasings for SNP pairs given read evidence, and clique potentials (e.g., $\phi_{v_{0,1}, v_{0,2}, v_{1,2}}$) capture phasing evidence from reads spanning three or more positions.

For any edge in E_Q representing three SNPs ℓ_0, ℓ_1, ℓ_2 for whom $\mathcal{R}_{\ell_0\ell_1\ell_2} = \emptyset$, we define $f(\phi_{\ell_0\ell_1\ell_2}) \propto 1 \forall \phi_{\ell_0\ell_1\ell_2} \in \Phi_{\ell_0\ell_1\ell_2}$. Informally, node and edge potentials represent unnormalized likelihoods of a read being generated conditioned on a particular haplotype phasing (See §A for the list of notations).

Inference algorithm leveraging the pCompass graph. The pCompass graph represents a probability distribution over haplotype assemblies. We perform inference using the pCompass graph using two algorithms: the Viterbi algorithm for maximum a posteriori (MAP) estimation and forward-filtering backward-sampling (FFBS) for posterior sampling and uncertainty quantification. To enable probabilistic inference on Q , we impose a topological ordering on the nodes of U according to ascending genomic position, first by the lesser-indexed of the two SNPs represented by a node, breaking ties by considering the second SNP. We then direct the edges of E_Q to respect this ordering. When the SNP graph contains multiple connected components, each component is ordered independently (see Appendix C and Appendix D for details).

Applying the matching algorithm to construct the full assembly. After applying Viterbi or FFBS to the pCompass graph, we obtain a local phasing $\phi_t \in \Phi_t$ for each node $u_t \in U$. However, these localphasings cannot be directly concatenated into a global haplotype solution H^* due to *haplotype label ambiguity*: since haplotypes are biologically unordered, any permutation of haplotype indices represents a valid solution. When two adjacent nodes $u_{\ell_0\ell_1}$ and $u_{\ell_1\ell_2}$ share position ℓ_1 , their phasings must be consistent at the shared position, but this consistency can be achieved through multiple different permutations of haplotype labels. We resolve this combinatorial matching problem through a greedy connectivity-based assembly approach (Algorithms E.1 and E.2) that incrementally selects the next variant to be phased and constructs the global haplotype configuration H^* variant by variant (Fig. E.1).

The variant selection algorithm maintains four sets: U^{phased} and U^{unphased} tracking which nodes in the SNP line graph Q have been processed, and S^{phased} and S^{unphased} tracking which SNP positions have been assigned to global haplotype H^* . The algorithm starts by selecting the first node in Q according to the topological order and assigning both of its positions using the node’s inferred phasing. At each iteration, we identify unphased nodes in Q that are adjacent to phased nodes U^{phased} , then we select the unphased position ℓ^* appearing in the most such nodes. Selecting positions with high connectivity ensures that the phasing decision is well-constrained by multiple node pairs in Q , progressively extending the phased region along paths of strong graph connectivity (Algorithm E.1 and §E.1).

The phasing position algorithm determines the haplotype assignment of a selected position ℓ^* through candidate generation and scoring. Candidates are constructed from nodes containing ℓ^* that are connected to already-phased positions, using node and edge potentials computed during graph construction. Each candidate must maintain consistency with the already-assigned alleles in $H^*[S^{\text{phased}}]$, i.e. the haplotype labels in S^{phased} are fixed, but the candidates may permute haplotype rows to achieve consistency at shared positions. Candidates are scored using a weighted combination of three criteria: likelihood (how well the candidate explains observed reads), minimum error correction (the number of sequence read allele corrections to map reads to the phasing), and inference agreement (consistency with Viterbi or FFBS results). After normalizing each metric within the candidate set, we select the highest-scoring candidate and assign its alleles for position ℓ^* to the global haplotype matrix H^* . When no valid candidates exist due to sparse coverage, we use the inferred phasing from any node containing ℓ^* (Algorithm E.2 and §E.2).

3.2 PHAPCOMPASS-long

Since the number of vertices in the SNP line graph grows quadratically with the length of a read, PHAPCOMPASS-short scales poorly with long sequence reads. Here, we introduce PHAPCOMPASS-long, a hierarchical haplotype mixture model whose complexity scales with the number of reads.

Defining the mixture model. The PHAPCOMPASS-long model describes how a read set \mathcal{R} is generated from a mixture of K conditional random fields (CRFs) h_k^* each representing a single haplotype along the genome (Fig. 3). Each haplotype CRF h_k^* is a chain over L variables w_1^k, \dots, w_L^k that each emit a single allele in $\{0, 1\}$ with 2 states per variable, one that emits a 0 allele with probability $1 - \varepsilon$ and another that emits a 0 allele

with probability ε , where $\varepsilon \in [0, 1]$ is the sequencing error rate. The read assignments, z_j , and hidden states, w_ℓ^k , are unobserved random variables. For convenience, define vector function $\epsilon(r[\ell]) = (\epsilon_0(r[\ell]), \epsilon_1(r[\ell]))$, where $\epsilon_a(r[\ell]) = 1 - \varepsilon$ if $r[\ell] = a$, and ε if $r[\ell] = a' \neq a$.

For each h_k^* , we compute the marginals as

$$\psi_\ell^k(a) \propto \prod_{\substack{r_j \in \mathcal{R}: \\ z_j = k \wedge r_j[\ell] \neq '-'}} \epsilon_a(r_j[\ell]),$$

and the transitions as

$$\psi_{\ell, \ell+1}^k(a_1, a_2) \propto \frac{|\{r_j \in \mathcal{R} : z_j = k \wedge r_j[\ell] = a_1 \wedge r_j[\ell+1] = a_2\}|}{|\{r_j \in \mathcal{R} : z_j = k \wedge r_j[\ell] \neq '-' \wedge r_j[\ell+1] \neq '-' \}|} + \delta,$$

where $\delta \geq 0$ is a hyperparameter used to smooth transition potentials.

To enforce genotype constraints, we define another chain-shaped conditional random field H^* over variables W_1, \dots, W_L , where each W_ℓ takes states over the 2^K configurations of $w_\ell^1, \dots, w_\ell^K$. The marginal potentials for each W_ℓ and transition potentials for each $W_\ell, W_{\ell+1}$ pair along H^* are defined by first taking the K -ary products over marginals and transitions from h_1^*, \dots, h_K^* , then only assigning non-zero mass to the states of W_ℓ that agree with the genotype as called in g_ℓ .

For a read r_j covering SNPs $\{\ell_0, \ell_0 + 1, \dots, \ell_0 + m_0\} \cup \{\ell_1, \dots, \ell_1 + m_1\} \cup \dots \cup \{\ell_d, \dots, \ell_d + m_d\}$, which is not necessarily contiguous for $\ell_0 < \dots < \ell_d$, we can define the conditional posterior probability of r_j given h_k^* , or colloquially the “likelihood” of r_j being emitted from h_k^* , as

$$\begin{aligned} P(r_j | h_k^*) = & \alpha_k(\ell_0) \cdot (\psi_{\ell_0}^k \cdot \epsilon(r_j[\ell_0])) \cdot \psi_{\ell_0, \ell_0+1}^k \cdot \dots \cdot \psi_{\ell_0+m_0-1, \ell_0+m_0}^k \cdot (\psi_{\ell_0+m_0}^k \cdot \epsilon(r_j[\ell_0 + m_0])) \\ & \cdot \psi_{\ell_1, \ell_1+1}^k \cdot \dots \cdot \psi_{\ell_1+m_1-1, \ell_1+m_1}^k \cdot \dots \\ & \cdot (\psi_{\ell_d}^k \cdot \epsilon(r_j[\ell_d])) \cdot \psi_{\ell_d, \ell_d+1}^k \cdot \dots \cdot \psi_{\ell_d+m_d-1, \ell_d+m_d}^k \cdot (\psi_{\ell_d+m_d}^k \cdot \epsilon(r_j[\ell_d + m_d])) \cdot \beta_k(\ell_d + m_d), \end{aligned} \quad (1)$$

where

- $\alpha_k(\ell_0)$ is the forward message into SNP ℓ_0 ,
- $\beta_k(\ell_d + m_d)$ is the backward message into SNP $\ell_d + m_d$,
- ψ_ℓ^k is the normalized marginal distribution over alleles for SNP ℓ , and
- $\psi_{\ell, \ell+1}^k$ is the transition probability between adjacent SNP variables ℓ and $\ell + 1$, normalized over source SNP ℓ ,

Intuitively, we first take the product of the emission probabilities for each observed state (i.e., SNP covered by the read) with the transition probabilities for each pair of states between the start and the end of the read (even if there is not observed allelic data on both ends of the transition). Then, we summarize the probability over unobserved alleles before the beginning and after the end of the read using the forward and backward messages respectively along the CRF to the read endpoints.

In the generative process, read assignments to haplotypes z_j are drawn uniformly from $\{1, \dots, K\}$, reads over a fixed set of SNPs are emitted from haplotypes $h_{z_j}^*$ as in Equation 1, and genotypes g_ℓ are emitted as the sum of alternate alleles represented in the phase of the state of variable W_ℓ . Notice that since w_ℓ^k and W_ℓ are parts of the undirected portion of the model, they have conditional distributions as described above, but are not *generated*.

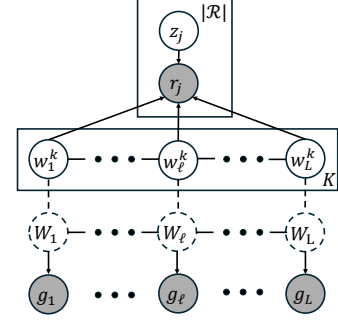


Fig. 3: **PHAPCOMPASS-long graphical model.** The dashed undirected edges from each w_ℓ^k to W_ℓ and around each W_ℓ represent a deterministic dependence between w_ℓ^k and W_ℓ (rather than statistical).

Gibbs sampling algorithm. To train the model, we develop an iterative algorithm inspired by the Levy *et al.* and Gibbs sampling algorithms [24]. We draw each $P(z_j = k | \cdot) \propto \frac{1}{K} \cdot P(r_j | h_k^*)$ and then update potentials for the two affected haplotype CRFs if the read assignment z_j has changed. To extract a complete haplotype assembly, we take a Viterbi path through H^* , concatenating the phasings per SNP as determined by the states for each W_ℓ along the path. Uncertainty quantification of the model is achieved by sampling multiple paths, such as using FFBS, through the CRF. During model training, we share information between separate h_k^* by augmenting the first 20 iterations of the Gibbs sampler with a gradient descent update on the potentials;

that is, we sample a single path using FFBS through the full CRF and take a linear combination of the existing potential distributions with the Dirac distribution of marginals and transitions defined by the single FFBS sample. We initialize each z_j randomly, and run the iterative algorithm until the log likelihood of the model, defined as $\log \left(\prod_{r_j \in \mathcal{R}} P(r_j | h_{z_j}^*) \right)$, converges. We remark that in PHAPCOMPASS-long, the likelihood of the genotype is omitted from the model likelihood because we strictly enforce its discrete consistency by nullifying atoms in W_ℓ inconsistent with g_ℓ .

4 Results

We evaluated PHAPCOMPASS, H-PoPG, WhatsHap, and HapTree-X on synthetic and experimental data with respect to haplotype assembly quality and uncertainty quantification.

4.1 Simulated data

We generated synthetic polyploid genomes from *S. tuberosum* reference haplotypes [35] using HaploSim [30]. For autopolyploids, we simulated ploidies in $\{2, 3, 4, 6\}$ with mutation rates $\mu \in \{0.001, 0.005, 0.01\}$ and 20 replicates per configuration. For allopolyploids, we generated structured subgenomes (AAB, AABB, AABCC) with inter-subgenome divergence $\mu_{\text{sub}} \in \{0.0001, 0.0005\}$ and within-subgenome variation $\mu_{\text{within}} \in \{0.00005, 0.0001\}$ (10 replicates per configuration). Paired-end 125bp short reads were simulated using ART with Illumina HiSeq 2500 profiles at coverages in $[3, 40]$ per haplotype [22]. Long reads were simulated using PBSIM3 with ONT R10.4 chemistry profiles (mean length $\sim 9kb$, Q13-14 base quality) with coverages in $[5, 40]$ per haplotype [31]. Reads were aligned using BWA-MEM (short) or Minimap2 (long), and fragments were extracted using Hap10 with base quality thresholds of Q13 and Q4 for short and long reads, respectively [27]. In total, we generated 1,200 autopolyploid short-read samples, 960 autopolyploid long-read samples, and 480 samples each for allopolyploid short and long reads (see §F, Table F.1, and Figs. F.2-F.9 for details).

4.2 Experimental data

Cultivated octoploid strawberry (*Fragaria x ananassa*) is an allopolyploid consisting of four subgenomes (A,B,C,D) originating from four diploid progenitor species. To benchmark allopolyploid haplotype assembly, raw *Fragaria x ananassa* reads were obtained from the European Nucleotide Archive (Biosample: SAMN13059213) [17]. Raw reads were subsequently adapter- and quality-trimmed using fastp v0.23.4 [8]. Duplicates were marked using picard v3.4.0 and the GATK MarkDuplicates v4.6.2.0 tool [28]. Subgenome A of the telomere-to-telomere *Fragaria x ananassa* ‘Seolhyang’ assembly [17] was extracted from the reference using samtools v1.20 [10]. Trimmed reads were then aligned to subgenome A using BWA-MEM v0.7.19 [25]. Alignments were sorted using samtools, and biallelic variants were called using the freebayes v1.3.10 with ploidy (-p) set to eight [16]. To reduce the effects of linkage disequilibrium, we thinned our VCF along static windows of 200 bp based on the estimated rate of linkage disequilibrium decay (120 bp) for cosmopolitan *F. x ananassa* [18]. We increased our window size to account for variability in linkage disequilibrium decay rates both along each chromosome and among homeologs, while maintaining sensitivity to attempt to detect local haplotype blocks (see §F.3 for additional data processing details).

4.3 Evaluation Criteria

To facilitate a fair comparison across both deterministic and probabilistic assemblers, we extend the commonly used evaluation metrics of minimum error correction (MEC) and vector error rate (VER) to accommodate the complexity associated with partially phased haplotype blocks and assembly uncertainty. Specifically, we extend the metrics used in prior works to consider the following scenarios observed in the output of polyploid assemblers:

1. the reconstructed phasing of a heterozygous SNP deviates from the ground truth genotype;
2. less than K haplotypes are assembled at a given SNP; and
3. the assembled haplotypes are not contiguous, but rather reported as a series of one or more “blocks”.

Generalized vector error rate. Given ground truth haplotypes, the vector error rate (VER) is the polyploid generalization of switch error for reconstructed phasings that obey genotype constraints. First, we define vector error for a contiguous and complete phasing. Let $H = \{h_1, \dots, h_K\}$ be the true phasing and $H^* = \{h_1^*, \dots, h_K^*\}$ be the reconstructed phasing, where each h_k and h_k^* are L -length vectors representing one true or phased haplotype. Let $\phi_\ell : \{1, \dots, K\} \rightarrow \{1, \dots, K\}$ be a bijection from the predicted phasing at SNP ℓ to the true phasing at SNP ℓ such that $h_k[\ell] = h_{\phi_\ell(k)}^*[\ell]$; that is, ϕ_ℓ maps 0 alleles to 0 alleles and 1 alleles to 1 alleles. There are $g[\ell]!(K - g[\ell])! = O(K!)$ such permutations that only exist when the genotype of the reconstruction matches the genotype of the ground truth; vector error is not well-defined for assemblies that do not respect the reported genotype. For the sake of comparison with assemblies that fail to align with genotype information, we perturb the computed assembly by introducing the minimal number of allele flips (chosen uniformly at random from the offending alleles) to make genotypes consistent and compute vector error rate on the modified assembly with a per flip penalty.

Let $\Phi = (\phi_1, \dots, \phi_L)$ be a sequence of valid matchings. We define the vector error associated with a matching of the entire reconstructed phasing as

$$\text{VE}(\Phi) = \sum_{\ell=2}^L |\{k : \phi_\ell(k) \neq \phi_{\ell-1}(k)\}|, \quad (2)$$

or the number of times that the matching “switches” which predicted haplotype maps to which true haplotype over the course of the assembly. The overall vector error for an assembly is then

$$\text{VE}(H, H^*) = \min_{\Phi} \{\text{VE}(\Phi)\}, \quad (3)$$

The vector error can be computed exactly using a dynamic program over transitions between valid matchings of adjacent SNPs in time $O(L(K!)^2)$. The vector error rate is defined as $\text{VER}(H, H^*) = \text{VE}(H, H^*)/L$.

Special considerations must be taken to compute a single VER for an assembly with many blocks. A block is a sub-assembly over which the phasing between all SNPs in the block is computed, such that the union of SNPs over all blocks is the disjoint union of $\{1, \dots, L\}$. Further, we define a block such that the number of haplotypes phased at each SNP within the block is constant. There exists four types of blocks: (1) fully phased (K haplotypes phased); (2) mostly phased ($K - 1$ haplotypes phased), which can be augmented with the final haplotype needed to respect the called genotype and treated as fully phased; (3) partially phased (between 1 and $K - 2$ haplotypes phased, inclusive); and (4) completely unphased.

We generalize vector error over multiple blocks by defining vector error for each block type and adding a penalty for each additional block reported beyond the first. The vector error for blocks of type 1 or 2 can be computed as described in Equations 2 and 3. The vector error for blocks of type 4 is computed as an expectation: we consider all of the valid bijections at each SNP position besides the first uniformly and compute the expected number of non-fixed points from an arbitrary but fixed permutation considered at the previous position, and sum over positions besides the first. The vector error for type 3 blocks is computed as a combination of the vector error (Equations 2 and 3) and expected vector error. See §F.4 for details on vector error computation for block types 3 and 4. Additionally, in order to report a single value, we penalize reconstructed phasings that phase into more than one block by computing the expected number of vectors errors “into” the first SNP of each additional block beyond the first using $K - \mathbb{I}\{g[\ell] > 1\} - \mathbb{I}\{K - g[\ell] > 1\}$. The vector error of an assembly is the sum of the within-block vector errors plus the additional block penalties.

Block-adjusted minimum error correction. The minimum error correction (MEC) criterion is often used when ground truth haplotypes are unknown. Traditionally, MEC measures the proportion of called alleles over all reads that have to be flipped for each read to map perfectly onto the reconstructed phasing. Formally,

$$\text{MEC}(\mathcal{R}, H^*) = \frac{1}{\sum_{r \in \mathcal{R}} |r|} \sum_{r \in \mathcal{R}} \min_{k \in \{1, \dots, K\}} \{d(r, h_k^*[r])\},$$

where $|r|$ is the number of alleles that read r covers, $d(u, v)$ is the Hamming distance between vectors u and v , and $h_k^*[r]$ is the k^{th} reconstructed haplotype at the set of SNPs that read r covers. The Hamming distance between an allele along a read and an unphased allele in the reconstruction is taken as 1, naturally giving the analog of MEC for partially phased blocks as long as the read is entirely contained within one phased block.

Because MEC considers the error correction over a *single* row of the reconstruction, we penalize each read that covers more than one block with the probability that the optimal haplotype chosen in each block is different for all covered blocks. So, for a read covering B blocks, we apply a penalty of $(B - 1) \cdot (1 - \frac{1}{K})$, or the expected number of times that the optimal haplotype for each pair of adjacent blocks differs, assuming single optimally matching haplotype for each block. Due to this penalty, the interpretation of MEC as a rate has to be loosened. A read covering B blocks as seen in isolation will contribute $O(B)$ to the block adjusted MEC, where in the single-block setting this is $O(1)$ as expected from the traditional definition of the metric.

4.4 Synthetic Data Results

We evaluated PHAPCOMPASS against three state-of-the-art polyploid haplotype assembly methods, WhatsHap, H-PoPG, and HapTree-X, using simulated data across multiple ploidies (2, 3, 4, 6), coverage depths ($3\times$ - $40\times$), and genomic structures (autopolyploid and allopolyploid). Performance was measured using the generalized VER and block-adjusted MEC. All results represent means across multiple replicates with shaded regions indicating standard error. WhatsHap and HapTree-X received VCF and BAM files, while H-PoPG and PHAPCOMPASS used fragment files extracted from the same alignments using Hap10’s extractHAIRS. Competing methods were run with default parameters as specified in their respective publications. For PHAPCOMPASS, we tuned hyperparameters using a separate autopolyploid validation dataset: with fixed mutation rate of 0.001, ploidy $\in \{2, 3, 4, 6\}$, 3 coverages ($5\times$, $10\times$, $20\times$), and 5 samples per configuration (60 samples in total). The selected parameters for PHAPCOMPASS-short were $w_F = 1/12$, $w_M = 10/12$, $w_L = 1/12$ (FFBS weight, MEC weight, likelihood weight respectively), and for PHAPCOMPASS-long were $\delta = 5$ (transition smoothing), $\varepsilon = 0.00001$ (error rate), and learning rate = 0.02 (gradient descent step size for FFBS augmentation). These parameters were held fixed across all test evaluations.

Autopolyploid genomes present the most challenging phasing scenario: all K haplotypes originate from the same ancestral species and accumulate mutations independently, creating scenarios where haplotypes can share long stretches of high similarity. This violates the fundamental assumption of most read clustering methods that similar reads originate from the same haplotype. Haplotype similarity heatmaps illustrate this challenge (Fig. F.3), which is coupled with larger SNP densities at lower mutation rates (Fig. F.2). In short-read autopolyploid data, the two probabilistic assemblers, HapTree-X and PHAPCOMPASS-short, demonstrated the lowest VER and MEC, though the latter specifically performs well in lower coverage and higher ploidy scenarios (Fig. 4a). HapTree-X did not complete execution on $K=6$ due to segmentation faults.

Long-read autopolyploid results show that PHAPCOMPASS-long maintained consistently low VER and MEC across all ploidies and coverages (Fig. 4b). The PHAPCOMPASS-long model iteratively refines both haplotype sequences and read assignments which enables the model to handle the ambiguities in autopolyploid long-read data, particularly in lower coverages where other methods performance drops.

Allopolyploid genomes differ from autopolyploids through subgenome divergence: haplotypes originating from different ancestral species accumulate systematic sequence differences that create structured heterozygosity. Even at low inter-subgenome mutation rates, haplotypes from different subgenomes showed Hamming distances of 0.85-0.95, while haplotypes within the same subgenome remained similar (Fig. F.7). On short-read allopolyploid data, all methods improved relative to autopolyploid performance, validating that subgenome divergence aids assembly (Fig. 4c). PHAPCOMPASS-short maintained lowest VER across ploidies and coverages, with particularly stable performance at $K=6$, even in lower coverages. HapTree-X achieved competitive performance at $K=6$, likely because its MEC objective aligns well with the distinct error signatures between divergent subgenomes.

Long-read allopolyploid results show convergence of top methods at high coverage, where abundant long-range information makes the problem well-constrained (Fig. 4d). However, performance diverged sharply at low coverage, where PHAPCOMPASS-long achieved the lowest VER and MEC. By sharing information between haplotypes via $\{W_\ell\}_{\ell=1}^L$, read coverage for some but not all haplotypes can be propagated to inform the phase of unobserved haplotype segments. Besides these criteria, block-level analysis reveals that PHAPCOMPASS produces fewer, longer phased blocks than competitors (Supplementary Figs. G.10 and G.13).

4.5 Uncertainty Quantification

An important feature of the PHAPCOMPASS probabilistic models is the ability to quantify uncertainty over phasings. The potential functions for both models imply an exponentially sized distribution over phasings,

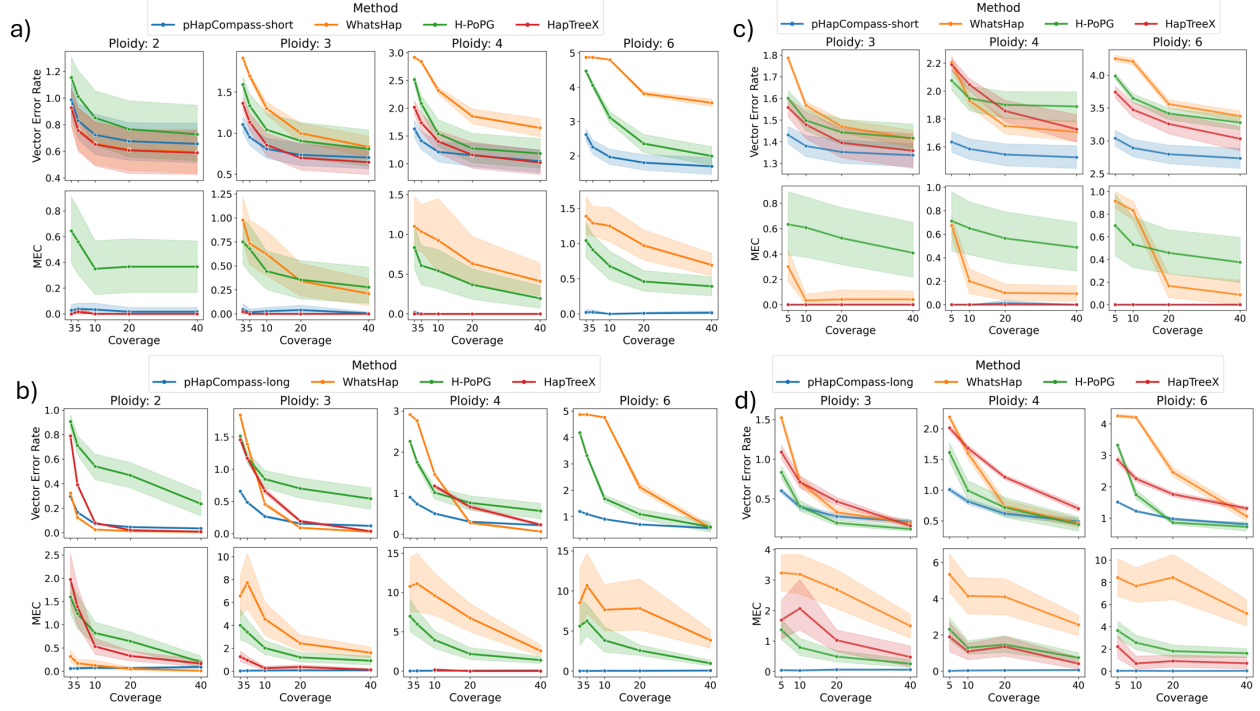


Fig. 4: **Haplotype assembly performance metrics across configurations.** (a-d) Vector Error Rate (top) and MEC (bottom) for pHAPCOMPASS (blue), WhatsHap (orange), H-PoPG (green), and HapTree-X (red) on: (a) autopolyploid short reads, (b) autopolyploid long reads, (c) allopolyploid short reads, (d) allopolyploid long reads.

which we approximate by collecting multiple FFBS samples. In pHAPCOMPASS-short, an FFBS path through the connected components (blocks) of Q corresponds to phasings over pairs of SNPs, joined using Algorithm E.2. In pHAPCOMPASS-long, a path through $H^* = (W_1, \dots, W_L)$ yields a single block assembly. In both models, the probability of a phasing is proportional to the number of consistent FFBS samples.

We evaluated uncertainty quantification by considering the phase between SNP pairs at different distances. After optimally matching the phasing samples to H , we computed the phase accuracy as the mean Hamming distance between each sample's phase to the ground truth, with Hamming distance extended to pairs of matrices in $\{0, 1\}^{K \times 2}$ as the number of elements in the matrices that differ. For example, a Hamming distance of 0 represents a perfect phase, and a Hamming distance of 2 represents two vector errors. The pair phase accuracy decreases (Hamming distance and uncertainty increases) as SNP distance increases before plateauing around a similar accuracy due to the evaluation of SNPs across blocks (Fig. 5). We remark that the difference in the asymptotes are due to Hamming distance being undefined for unassembled SNPs and pHAPCOMPASS-short assembling fewer SNPs than pHAPCOMPASS-long.

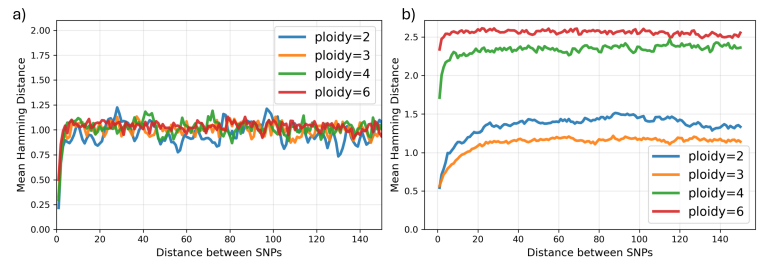


Fig. 5: **Uncertainty quantification via FFBS sampling.** Mean Hamming distance versus SNP distance for (a) pHAPCOMPASS-short and (b) pHAPCOMPASS-long across ploidies.

4.6 Experimental Data Results

To evaluate performance on experimental data, we applied PHAPCOMPASS-short, WhatsHap, and H-PoPG to octoploid strawberry data at two coverage levels $8\times$ and $16\times$. We filtered variants along 200 bp windows to reduce linkage disequilibrium effects and extracted chromosome regions for assembly (Table H.2). PHAPCOMPASS-short achieved lower MEC than competing methods, indicating assemblies with minimal read-haplotype conflicts. Additionally, it produced fewer phased blocks compared to WhatsHap and H-PoPG, demonstrating the continuity across longer genomic segments even with short-read data, where clustering-based methods make different blocks due to ambiguous read assignments (Tables H.3 and H.4).

5 Discussion

The evaluation of PHAPCOMPASS on realistic autopolyploid and allopolyploid genomes suggests several key insights. First, realistic simulation exposes fundamental limitations of clustering-based methods that depends only on read similarity. Second, PHAPCOMPASS’s probabilistic framework, which models uncertainty in both haplotype configurations and read assignments, provides robust performance across the full spectrum of polyploid structures, ploidies, and coverage regimes. Third, the distinction between autopolyploidy and allopolyploidy proves critical for understanding assembly performance. Allopolyploid subgenome divergence creates structured heterozygosity that aids all methods, however, PHAPCOMPASS maintains a consistent advantage across both genomic structures, suggesting that the probabilistic framework provides value beyond simply exploiting subgenome divergence. Fourth, the convergence of methods at high coverage in allopolyploid long-read data indicates that when evidence is abundant and subgenomes are divergent, the problem becomes well-constrained for multiple algorithmic approaches. The divergence at low coverage reveals the value of probabilistic inference: maintaining distributions over phasings enables PHAPCOMPASS-long to integrate sparse evidence optimally, while greedy methods commit irreversibly to early decisions based on insufficient data. The reduced block counts for PHAPCOMPASS relative to competitors demonstrate that this connectivity-based approach maintains phasing continuity.

Limitations of the current work suggest directions for future development. The hyperparameter tuning for PHAPCOMPASS used a separate validation set with fixed mutation rate, which may not generalize optimally to all experimental conditions. The matching algorithm’s greedy selection strategy, while effective, does not guarantee global optimality. The computational requirements of PHAPCOMPASS-short and PHAPCOMPASS-long are driven by different factors (§I and Fig. I.14). PHAPCOMPASS-short scales well for short reads, but the SNP line graph becomes too dense for long read data. The runtime for PHAPCOMPASS-long is dominated by the iterative Gibbs sampling algorithm, which limits scalability for high coverage data. In both cases, algorithmic improvements like approximating exponentially sized factors or variational inference algorithms could be used to improve scalability for PHAPCOMPASS-short and PHAPCOMPASS-long, respectively. Due to these computational differences, we evaluate each method on its intended data type.

6 Conclusions

In this work, we made contributions to the evaluation, simulation, and computation of polyploid genome assemblies. First, we extended the VER and block-adjusted MEC evaluation criteria to handle the complexities of polyploid assemblies: partial phasing, multiple blocks, and non-complementary haplotypes. Second, We developed a pipeline for realistic polyploid genome simulation, which captures the true similarity structure that makes polyploid phasing fundamentally challenging; both the software and simulated datasets for both autopolyploid and allopolyploid genomes are freely available to the community to facilitate benchmarking of future polyploid assembly methods [21]. Lastly, we presented pHapCompass, a probabilistic framework for polyploid haplotype assembly that explicitly models and quantifies uncertainty in both haplotype phase and read-to-haplotype assignments. PHAPCOMPASS demonstrated reliable performance across diverse polyploid configurations, with particular advantages in low-coverage scenarios where deterministic methods fail. Unlike existing polyploid assemblers that output single point estimates, PHAPCOMPASS uses FFBS to generate distributions over haplotype configurations. Each sample represents a plausible phasing weighted by its posterior probability given the observed reads, which we report in the VCF formatted output, which includes probability scores for each generated phasing.

References

1. Omar Abou Saada, Andreas Tsouris, Chris Eberlein, Anne Friedrich, and Joseph Schacherer. nphase: an accurate and contiguous phasing method for polyploids. *Genome biology*, 22(1):126, 2021.
2. Derek Aguiar and Sorin Istrail. Hapcompass: A fast cycle basis algorithm for accurate haplotype assembly of sequence data. *Journal of Computational Biology*, 19(6):577–590, June 2012.
3. Derek Aguiar and Sorin Istrail. Haplotype assembly in polyploid genomes and identical by descent shared tracts. *Bioinformatics*, 29(13):i352–i360, 2013. *also in proceedings of ISMB 2013*.
4. Vikas Bansal and Vineet Bafna. Hapcut: an efficient and accurate algorithm for the haplotype assembly problem. *Bioinformatics*, 24(16):i153–i159, 2008.
5. Emily Berger, Deniz Yorukoglu, Jian Peng, and Bonnie Berger. Haptree: a novel bayesian framework for single individual polyplootyping using ngs data. *PLoS computational biology*, 10(3):e1003502, 2014.
6. Emily Berger, Deniz Yorukoglu, Lillian Zhang, Sarah K. Nyquist, Alex K. Shalek, Manolis Kellis, Ibrahim Numanagić, and Bonnie Berger. Improved haplotype inference by exploiting long-range linking and allelic imbalance in rna-seq datasets. *Nature Communications*, 11(1):4662, Sep 2020.
7. Sharon R Browning and Brian L Browning. Haplotype phasing: existing methods and new developments. *Nature Reviews Genetics*, 12(10):703–714, 2011.
8. Shifu Chen, Yanqing Zhou, Yaru Chen, and Jia Gu. fastp: an ultra-fast all-in-one fastq preprocessor. *Bioinformatics*, 34(17):i884–i890, 2018.
9. Shorya Consul, Ziqi Ke, and Haris Vikalo. Xhap: haplotype assembly using long-distance read correlations learned by transformers. *Bioinformatics Advances*, 3(1):vbadi169, 2023.
10. Petr Danecek, James K Bonfield, Jennifer Liddle, John Marshall, Valeriu Ohan, Martin O Pollard, Andrew Whitwham, Thomas Keane, Shane A McCarthy, Robert M Davies, et al. Twelve years of samtools and bcftools. *Gigascience*, 10(2):giab008, 2021.
11. Shreepriya Das and Haris Vikalo. Sdhap: haplotype assembly for diploids and polyploids via semi-definite programming. *BMC genomics*, 16:1–16, 2015.
12. Mark J Dunning, Mike L Smith, Matthew E Ritchie, and Simon Tavaré. beadarray: R classes and methods for illumina bead-based data. *Bioinformatics*, 23(16):2183–2184, 2007.
13. Peter Edge, Vineet Bafna, and Vikas Bansal. Hapcut2: robust and accurate haplotype assembly for diverse sequencing technologies. *Genome research*, 27(5):801–812, 2017.
14. Gilad D Evrony, Anjali Gupta Hinch, and Chongyuan Luo. Applications of single-cell dna sequencing. *Annual review of genomics and human genetics*, 22:171, 2021.
15. Philip Ewels, Måns Magnusson, Sverker Lundin, and Max Käller. Multiqc: summarize analysis results for multiple tools and samples in a single report. *Bioinformatics*, 32(19):3047–3048, 2016.
16. Erik Garrison and Gabor Marth. Haplotype-based variant detection from short-read sequencing. *arXiv preprint arXiv:1207.3907*, 2012.
17. Hyeondae Han, Yoon Jeong Jang, Koeun Han, Han-Na Park, Do-Sun Kim, Seonghee Lee, and Youngjae Oh. Chromosome-level genome assembly of cultivated strawberry ‘seolhyang’(fragaria × ananassa). *Scientific Data*, 12(1):1002, 2025.
18. Michael A Hardigan, Anne Lorant, Dominique DA Pincot, Mitchell J Feldmann, Randi A Famula, Charlotte B Acharya, Seonghee Lee, Sujeet Verma, Vance M Whitaker, Nahla Bassil, et al. Unraveling the complex hybrid ancestry and domestication history of cultivated strawberry. *Molecular biology and evolution*, 38(6):2285–2305, 2021.
19. Dan He, Subrata Saha, Richard Finkers, and Laxmi Parida. Efficient algorithms for polyploid haplotype phasing. *BMC genomics*, 19(Suppl 2):110, 2018.
20. Robin J Hofmeister, Diogo M Ribeiro, Simone Rubinacci, and Olivier Delaneau. Accurate rare variant phasing of whole-genome and whole-exome sequencing data in the uk biobank. *Nature genetics*, 55(7):1243–1249, 2023.
21. Marjan Hosseini, Ella Veiner, Thomas Bergendahl, Tala Yassenpoor, Zane Smith, Margaret Staton, and Derek Aguiar. pHapCompass: Probabilistic Polyploid Haplotype Assembly. <https://github.com/bayesomicslab/pHapCompass>, 2025.
22. Weichun Huang, Leping Li, Jason R Myers, and Gabor T Marth. Art: a next-generation sequencing read simulator. *Bioinformatics*, 28(4):593–594, 2012.
23. Giuseppe Lancia, Vineet Bafna, Sorin Istrail, Ross Lippert, and Russell Schwartz. Snps problems, complexity, and algorithms. In *European symposium on algorithms*, pages 182–193. Springer, 2001.
24. Samuel Levy, Granger Sutton, Pauline C Ng, Lars Feuk, Aaron L Halpern, Brian P Walenz, Nelson Axelrod, Jiaqi Huang, Ewen F Kirkness, Gennady Denisov, Yuan Lin, Jeffrey R MacDonald, Andy Wing Chun W Pang, Mary Shago, Timothy B Stockwell, Alexia Tsiamouri, Vineet Bafna, Vikas Bansal, Saul A Kravitz, Dana a Busam, Karen Y Beeson, Tina C McIntosh, Karin A Remington, Josep F Abril, John Gill, Jon Borman, Yu-Hui H Rogers, Marvin E Frazier, Stephen W Scherer, Robert L Strausberg, and J Craig Venter. The diploid genome sequence of an individual human. *PLoS biology*, 5(10):e254+, sep 2007.

25. Heng Li and Richard Durbin. Fast and accurate short read alignment with Burrows-Wheeler transform. *Bioinformatics*, 25(14):1754–1760, 2009.
26. Junwei Luo, Jiaojiao Wang, Jingjing Wei, Chaokun Yan, and Huimin Luo. Deephapnet: a haplotype assembly method based on retnet and deep spectral clustering. *Briefings in Bioinformatics*, 26(1):bbae656, 12 2024.
27. Sina Majidian, Mohammad Hossein Kahaei, and Dick De Ridder. Hap10: reconstructing accurate and long polyploid haplotypes using linked reads. *BMC bioinformatics*, 21(1):253, 2020.
28. Aaron McKenna, Matthew Hanna, Eric Banks, Andrey Sivachenko, Kristian Cibulskis, Andrew Kernytsky, Kiran Garimella, David Altshuler, Stacey Gabriel, Mark Daly, and Mark A DePristo. The Genome Analysis Toolkit: A MapReduce framework for analyzing next-generation DNA sequencing data. *Genome Research*, 20(9):1297–1303, sep 2010.
29. M-Hossein Moeinzadeh, Jun Yang, Evgeny Muzychenko, Giuseppe Gallone, David Heller, Knut Reinert, Stefan Haas, and Martin Vingron. Ranbow: a fast and accurate method for polyploid haplotype reconstruction. *PLOS Computational Biology*, 16(5):e1007843, 2020.
30. Ehsan Motazed, Richard Finkers, Chris Maliepaard, and Dick de Ridder. Exploiting next-generation sequencing to solve the haplotyping puzzle in polyploids: a simulation study. *Briefings in Bioinformatics*, 19(3):387–403, 01 2017.
31. Yukiteru Ono, Michiaki Hamada, and Kiyoshi Asai. Pbsim3: a simulator for all types of pacbio and ont long reads. *NAR genomics and bioinformatics*, 4(4):lqac092, 2022.
32. Sven D Schrinner, Rebecca Serra Mari, Jana Ebler, Mikko Rautiainen, Lancelot Seillier, Julia J Reimer, Björn Usadel, Tobias Marschall, and Gunnar W Klau. Haplotype threading: accurate polyploid phasing from long reads. *Genome biology*, 21:1–22, 2020.
33. Russell Schwartz. Theory and Algorithms for the Haplotype Assembly Problem. *Commun. Inf. Syst.*, 10(1):23–38, 2010.
34. Andrews Simon et al. Fastqc: a quality control tool for high throughput sequence data. *Version 0.10*, 1, 2010.
35. Hequan Sun, Wen-Biao Jiao, José A. Campoy, Kristin Krause, Manish Goel, Kat Folz-Donahue, Christian Kukat, Bruno Huettel, and Korbinian Schneeberger. Chromosome-scale and haplotype-resolved genome assembly of a tetraploid potato cultivar. *bioRxiv*, 2021.
36. Yves Van de Peer, Eshchar Mizrahi, and Kathleen Marchal. The evolutionary significance of polyploidy. *Nature Reviews Genetics*, 18(7):411–424, 2017.
37. Minzhu Xie, Qiong Wu, Jianxin Wang, and Tao Jiang. H-pop and h-popg: heuristic partitioning algorithms for single individual haplotyping of polyploids. *Bioinformatics*, 32(24):3735–3744, 2016.

A Notation

Indices

- j : Read index, $j \in \{1, \dots, |\mathcal{R}|\}$
- ℓ : SNP position index, $\ell \in \{1, \dots, L\}$
- k : Haplotype index, $k \in \{1, \dots, K\}$

Problem Setup

- K : Ploidy level (number of haplotypes)
- L : Total number of heterozygous SNP positions
- $\mathcal{R} = \{r^{(1)}, r^{(2)}, \dots, r^{(|\mathcal{R}|)}\}$: Set of sequencing reads
- $\mathcal{G} = \{g_1, \dots, g_L\}$: Reference genotype information, where $g_\ell \in \{0, \dots, K\}$ is the count of alternate alleles at position ℓ .
- $H = \{h^{(1)}, \dots, h^{(K)}\}$: Set of K haplotypes to be reconstructed (ground truth).
- $H^* = \{h^{(1)}, \dots, h^{(K)}\}$: Set of K predicted haplotypes.
- $h^{(k)}[\ell] \in \{0, 1\}$: Allele of haplotype k at position ℓ (0=reference, 1=alternate)
- ε : Sequencing error rate.

Graphs

- $G = (V, E)$: **SNP graph**, where $V = \{1, \dots, L\}$ are SNP positions and $(\ell_0, \ell_1) \in E$ if at least one read covers both positions
- $Q = (U, E_Q)$: **Line graph of G** , where each node $u_{\ell_0 \ell_1} \in U$ represents an edge $(\ell_0, \ell_1) \in E$, and two nodes in U are adjacent in E_Q if their corresponding edges in G share exactly one SNP
- $Q' = (U, E'_Q)$: **Directed acyclic graph (DAG)** derived from Q by directing edges according to SNP order

Phasings

- $\phi_{\ell_0 \ell_1} \in \{0, 1\}^{K \times 2}$: A **phasing configuration** for two SNPs ℓ_0 and ℓ_1 , represented as a $K \times 2$ binary matrix where row k contains the alleles of haplotype k at positions ℓ_0 and ℓ_1
- $\phi_{\ell_0 \ell_1}^{(k)} \in \{0, 1\}^2$: The k -th row of phasing $\phi_{\ell_0 \ell_1}$, representing the allele pair from haplotype k
- $\phi_{\ell_0 \ell_1}^{(k)}(\ell)$: The allele at position ℓ in haplotype k within phasing $\phi_{\ell_0 \ell_1}$
- $\Phi_{\ell_0 \ell_1} \subset \{0, 1\}^{K \times 2}$: The **space of valid phasings** for SNPs ℓ_0 and ℓ_1 that satisfy genotype constraints
- $\phi_{\ell_0 \ell_1 \ell_2} \in \{0, 1\}^{K \times 3}$: A phasing configuration for three SNPs ℓ_0 , ℓ_1 , and ℓ_2
- $\Phi_{\ell_0 \ell_1 \ell_2} \subset \{0, 1\}^{K \times 3}$: The space of valid phasings for three SNPs

Read Sets

- $\mathcal{R}_{\ell_0 \ell_1} = \{r \in \mathcal{R} : r[\ell_0] \neq '-' \wedge r[\ell_1] \neq '-'\}$: Set of reads covering both SNP positions ℓ_0 and ℓ_1
- $\mathcal{R}_{\ell_0 \ell_1 \ell_2} = \{r \in \mathcal{R} : r[\ell_0] \neq '-' \wedge r[\ell_1] \neq '-' \wedge r[\ell_2] \neq '-'\}$: Set of reads covering all three SNP positions

Likelihood and Potentials

- $d(\cdot, \cdot)$: Hamming distance between two binary vectors
- $\mathcal{L}(r, \phi_{\ell_0 \ell_1})$: Likelihood of observing read r given phasing $\phi_{\ell_0 \ell_1}$
- $f(\phi_{\ell_0 \ell_1})$: **Node potential** (emission probability) for phasing $\phi_{\ell_0 \ell_1}$, computed as the sum of likelihoods over all reads in $\mathcal{R}_{\ell_0 \ell_1}$
- $f(\phi_{\ell_0 \ell_1 \ell_2})$: **Edge potential** (transition probability) for three-SNP phasing $\phi_{\ell_0 \ell_1 \ell_2}$

B Enumerating Valid Phasings for Two SNPs

Consider a tetraploid organism ($K = 4$) with genotypes $g_\ell = 2$ and $g_{\ell'} = 2$ at two adjacent SNP positions ℓ and ℓ' .

Each haplotype can have one of four possible allele patterns at these two positions:

- $(0, 0)$: reference allele at both positions
- $(0, 1)$: reference at ℓ , alternate at ℓ'
- $(1, 0)$: alternate at ℓ , reference at ℓ'
- $(1, 1)$: alternate allele at both positions

A phasing configuration is characterized by the count vector $\mathbf{t} = [t_{00}, t_{01}, t_{10}, t_{11}]$, where t_{ab} denotes the number of haplotypes with pattern (a, b) .

Genotype constraints. These counts must satisfy:

$$\begin{aligned} t_{10} + t_{11} &= g_\ell = 2 && \text{(total 1's at position } \ell) \\ t_{01} + t_{11} &= g_{\ell'} = 2 && \text{(total 1's at position } \ell') \\ t_{00} + t_{01} + t_{10} + t_{11} &= K = 4 && \text{(total haplotypes)} \\ t_{ab} &\geq 0 \quad \forall a, b && \text{(non-negativity)} \end{aligned}$$

Parameterization. We parameterize by t_{11} , the count of $(1, 1)$ patterns. Given t_{11} , the other counts are determined:

$$t_{10} = g_\ell - t_{11} = 2 - t_{11} \tag{4}$$

$$t_{01} = g_{\ell'} - t_{11} = 2 - t_{11} \tag{5}$$

$$t_{00} = K - g_\ell - g_{\ell'} + t_{11} = 4 - 2 - 2 + t_{11} = t_{11} \tag{6}$$

Feasible range. For all counts to be non-negative:

$$t_{11} \geq 0 \tag{7}$$

$$t_{10} = 2 - t_{11} \geq 0 \implies t_{11} \leq 2 \tag{8}$$

$$t_{01} = 2 - t_{11} \geq 0 \implies t_{11} \leq 2 \tag{9}$$

$$t_{00} = t_{11} \geq 0 \implies t_{11} \geq 0 \tag{10}$$

Thus $t_{11} \in \{0, 1, 2\}$, yielding exactly **three valid phasings**:

t_{11}	t_{00}	t_{01}	t_{10}	\mathbf{t}	Phasing Configuration
0	0	2	2	$[0, 2, 2, 0]$	$\begin{bmatrix} 0 & 1 \\ 0 & 1 \\ 1 & 0 \\ 1 & 0 \end{bmatrix}$
1	1	1	1	$[1, 1, 1, 1]$	$\begin{bmatrix} 0 & 0 \\ 0 & 1 \\ 1 & 0 \\ 1 & 1 \end{bmatrix}$
2	2	0	0	$[2, 0, 0, 2]$	$\begin{bmatrix} 0 & 0 \\ 0 & 0 \\ 1 & 1 \\ 1 & 1 \end{bmatrix}$

Each row in the phasing configuration matrix corresponds to one haplotype, with columns representing the two SNP positions.

Verification. For $t_{11} = 1$ (middle row):

- Count of 1's at position ℓ (first column): $0 + 0 + 1 + 1 = 2 = g_\ell$
- Count of 1's at position ℓ' (second column): $0 + 1 + 0 + 1 = 2 = g_{\ell'}$
- Total haplotypes: $1 + 1 + 1 + 1 = 4 = K$

General case. For arbitrary genotypes $(g_\ell, g_{\ell'})$ and ploidy K , the feasible range is:

$$t_{11} \in [\max(0, g_\ell + g_{\ell'} - K), \min(g_\ell, g_{\ell'})]$$

The number of valid phasings is therefore:

$$|\Phi_{\ell\ell'}| = \min(g_\ell, g_{\ell'}) - \max(0, g_\ell + g_{\ell'} - K) + 1 = O(K)$$

This represents a reduction from the $2^{2K} = 2^8 = 256$ possible binary matrices without genotype constraints.

C Viterbi Details

The Viterbi algorithm computes the maximum a posteriori (MAP) sequence of states in the directed pHapCompass graph $Q' = (U, E'_Q)$:

$$(\phi_1^*, \dots, \phi_{|U|}^*) = \arg \max_{\phi_1, \dots, \phi_{|U|}} P(\phi_1, \dots, \phi_{|U|} \mid \mathcal{R}).$$

This is solved via dynamic programming. For each node $u_t \in U$ and state $\phi_t \in \Phi_t$, we compute:

$$V_t(\phi_t) = \max_{\phi_1, \dots, \phi_{t-1}} P(\phi_1, \dots, \phi_t, \mathcal{R}_{1:t}),$$

the maximum probability of any path ending in state ϕ_t given all observations up to node t , where $\mathcal{R}_{1:t}$ denotes all reads covering SNP pairs in nodes u_1, \dots, u_t .

Base Case ($t = 1$)

$$V_1(\phi_1) = P(\phi_1) \prod_{r \in \mathcal{R}_{\ell_0 \ell_1}} L(r, \phi_1),$$

where $P(\phi_1)$ is the prior probability of phasing ϕ_1 (uniform), and $L(r, \phi_1)$ is the likelihood from Equation (2).

Recursion ($t = 2, \dots, |U|$)

$$V_t(\phi_t) = \left(\prod_{r \in \mathcal{R}_t} L(r, \phi_t) \right) \times \max_{\phi_{Pa(u_t)}} \left[\prod_{u_p \in Pa(u_t)} V_p(\phi_p) \times P(\phi_t \mid \phi_{Pa(u_t)}) \right],$$

where:

- \mathcal{R}_t is the set of reads covering the SNP pair at node u_t
- $Pa(u_t)$ denotes the parent nodes of u_t in the directed graph Q'
- $\phi_{Pa(u_t)}$ denotes the collection of parent phasings
- $P(\phi_t \mid \phi_{Pa(u_t)})$ is the transition probability derived from edge potentials (Equation 3), normalized over all three-SNP phasings consistent with parent states

The recursion proceeds in topological order. At each step, the maximizing parent configuration is recorded via a backpointer to reconstruct the optimal path after completion. Each connected component of Q is processed independently.

D FFBS Details

We direct the edges of the pHapCompass graph $Q = (U, E_Q)$ to obtain $Q' = (U, E'_Q)$ by imposing a topological ordering on nodes according to ascending genomic position. Each vertex $u_{\ell_0 \ell_1} \in U$ has state space $\Phi_{\ell_0 \ell_1}$.

The forward-filtering backward-sampling algorithm computes forward messages in topological order, then samples states in reverse order.

Forward Pass The forward message for each vertex u_t represents the joint probability of state ϕ_t and all observations up to node t :

$$\alpha_t(\phi_t) = P(\phi_t, \mathcal{R}_{1:t}),$$

where $\mathcal{R}_{1:t}$ denotes all reads covering SNP pairs in nodes u_1, \dots, u_t .

Base Case ($t=1$):

$$\alpha_1(\phi_1) = P(\phi_1) \prod_{r \in \mathcal{R}_{\ell_0 \ell_1}} L(r, \phi_1),$$

where $P(\phi_1)$ is the prior (uniform) and $L(r, \phi_1)$ is the likelihood defined in Equation (2).

Recursion ($t = 2, \dots, |U|$):

$$\begin{aligned}\alpha_t(\phi_t) &= P(\phi_t, \mathcal{R}_{1:t}) \\ &= \prod_{r \in \mathcal{R}_t} L(r, \phi_t) \sum_{\phi_{Pa(u_t)}} P(\phi_t \mid \phi_{Pa(u_t)}) \prod_{u_p \in Pa(u_t)} \alpha_p(\phi_p),\end{aligned}\tag{11}$$

where:

- \mathcal{R}_t is the set of reads covering the SNP pair at node u_t
- $L(r, \phi_t)$ is the emission probability from Equation (2)
- $P(\phi_t \mid \phi_{Pa(u_t)})$ is the transition probability derived from edge potentials in Equation (3), normalized over all three-SNP phasings consistent with parent states
- $Pa(u_t)$ denotes the parent nodes of u_t in the directed graph Q'

Forward messages are computed only after all parent messages are available, following the topological order.

Backward Sampling We sample states sequentially in reverse topological order from the posterior distribution $P(\phi_{1:|U|} \mid \mathcal{R})$.

Base Case ($t=|U|$):

Sample the final node proportional to its normalized forward message:

$$\phi_{|U|} \sim \frac{\alpha_{|U|}(\phi_{|U|})}{\sum_{\phi'_{|U|}} \alpha_{|U|}(\phi'_{|U|})}.$$

Recursion ($t = |U|-1, \dots, 1$):

For each node u_t , sample from the conditional posterior given all sampled children:

$$P(\phi_t \mid \{\phi_c : u_c \in Ch(u_t)\}, \mathcal{R}) \propto \alpha_t(\phi_t) \prod_{u_c \in Ch(u_t)} P(\phi_c \mid \phi_t),$$

where $Ch(u_t)$ denotes the children of u_t in Q' . Each node is sampled only after all its children have been sampled, proceeding in reverse topological order. Each connected component of Q is processed independently.

E Matching Problem

E.1 Variant Selection Algorithm

The variant selection algorithm (Algorithm E.1) constructs a final haplotype solution by iteratively selecting one variant to be phased at a time, using a greedy connectivity-based strategy. The algorithm maintains four sets throughout execution:

- U^{phased} : nodes in Q whose phasings have been incorporated into the global solution
- U^{unphased} : nodes in Q not yet processed
- S^{phased} : individual SNP positions that have been assigned to global haplotype rows
- S^{unphased} : SNP positions not yet assigned

Note that a node $u_{\ell_0 \ell_1} \in U$ represents a pair of SNP positions, while elements of S are individual positions. A node is considered phased or processed once both of its positions have been assigned to the final haplotype matrix, or once it has been used to constrain the phasing of its positions.

Initialization (Lines 2-7). The algorithm begins with all four sets initialized appropriately: the phased sets are empty, and the unphased sets contain all nodes and all positions, respectively. Block identifiers track which positions belong to the same connected component, starting with `block_id = 1`.

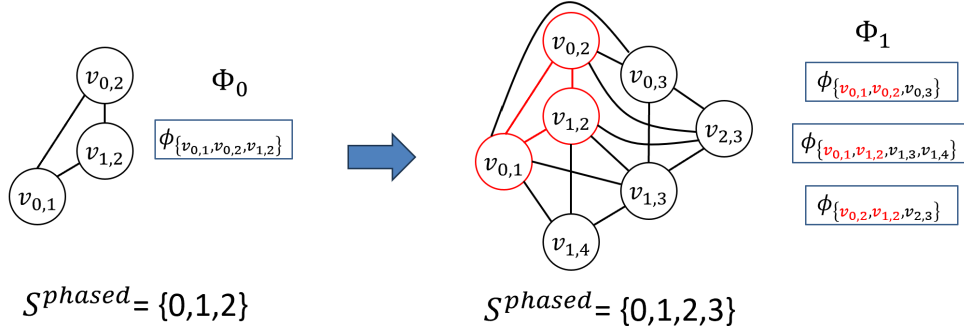


Fig.E.1: **Variant selection algorithm example.** Initially $U^{\text{phased}} = v_{0,1}$. Then the variant selection algorithm selects position $\ell^* = 2$ with maximum connectivity (2 edges) to already-phased nodes U^{phased} . The phasing is done in the phasing space of Φ_0 covering positions $\{0,1,2\}$ (left). After phasing position 2, the algorithm updates $U^{\text{phased}} = \{v_{0,1}, v_{0,2}, v_{1,2}\}$ and $S^{\text{phased}} = \{0,1,2\}$ (middle). Then we the next highest-connectivity position $\ell^* = 3$ with 6 edges compared to 4 with 2 edges. Please note that the phasing space now has changed to Φ_1 (right).

Starting node selection (Lines 8-13). To begin phasing, we select the first node $u_{\ell_0\ell_1}$ according to the topological ordering of Q (typically the leftmost pair in genomic coordinates). We assign both positions ℓ_0 and ℓ_1 to the global haplotype matrix H^* using the inferred phasing $\phi_{u_{\ell_0\ell_1}}^*$ obtained from either Viterbi or FFBS. The notation ϕ_u^* denotes the best or sampled phasing for node u : for Viterbi, this is the most probable state; for FFBS, this is a sample from the posterior distribution. Both positions are marked as phased, the node is moved from U^{unphased} to U^{phased} , and both positions are assigned to the current block.

Main loop (Lines 14-34). The algorithm continues until all positions have been phased ($S^{\text{unphased}} = \emptyset$).

Finding neighbor nodes (Line 16). At each iteration, we identify the set \mathcal{N} of unphased nodes that are adjacent (in the graph Q) to at least one of the nodes in the phased node set (U^{phased}). These are the nodes that can be used to extend the current phased set, as they connect already-phased positions to new positions.

Handling disconnected components (Lines 18-25). If $\mathcal{N} = \emptyset$, no unphased nodes connect to the current phased set, indicating that we have exhausted the current connected component of Q . In this case, we increment the block identifier to start a new phasing block, select the next unphased node $u_{\ell_i\ell_j}$ in topological order, initialize its phasing using $\phi_{u_{\ell_i\ell_j}}^*$, update all four sets accordingly, and continue to the next iteration. Positions in different blocks are phased independently and may have inconsistent haplotype labelings across blocks.

Selecting the next position (Lines 27-31). If neighbor nodes exist, we select the next position to phase based on connectivity. For each unphased position ℓ that appears in at least one node in \mathcal{N} , we compute its connectivity as the number of nodes in \mathcal{N} containing ℓ . The position ℓ^* with maximum connectivity is selected, as it has the most connection to the already-phased set.

Phasing the selected position (Line 33). The PHASEPOSITION subroutine (Algorithm E.2) is called to determine the haplotype assignment $\mathbf{h}_{\ell^*} \in \{0,1\}^K$ for position ℓ^* . This subroutine generates and scores candidate phasings based on read evidence, genotype constraints, and agreement with the inferred phasings $\{\phi_u^*\}$. The inputs include: the selected position ℓ^* , the set of phased positions S^{phased} , the current global haplotype matrix \mathcal{H} , the set of neighbor nodes \mathcal{N} , the inferred phasings $\{\phi_u^*\}$, and the set of reads \mathcal{R} .

Updating the global solution (Lines 35-40). The selected haplotype column \mathbf{h}_{ℓ^*} is assigned to position ℓ^* in the global matrix. P Position ℓ^* is moved from S^{unphased} to S^{phased} and assigned to the current block. Finally, all nodes in \mathcal{N} that contain position ℓ^* are moved from U^{unphased} to U^{phased} , as these nodes have now been fully utilized in the phasing process.

Termination and output (Line 42). The algorithm terminates when $S^{\text{unphased}} = \emptyset$, meaning all positions have been phased. The output consists of the global haplotype matrix $H^* \in \{0, 1, ' -'\}^{K \times L}$ and the block assignment vector $\mathbf{b} \in (\mathbb{N} \cup \{\text{NaN}\})^L$, where $\mathbf{b}[\ell]$ indicates which phasing block contains position ℓ . Positions that were not covered by any reads remain unphased and can be assigned NaN in the block vector, though in practice we assign them to the nearest block or use genotype-based imputation.

Note on unphased positions. In practice, positions not covered by any informative reads, remain unphased by the algorithm. These positions can be assigned $\mathbf{b}[\ell] = \text{NaN}$ to indicate missing phase information, similarly for such variants, $H^*[\cdot, \ell] = ' -'$.

Algorithm E.1 Variant Selection Algorithm

Require: SNP Line Graph $Q = (U, E_Q)$, inferred phasings $\{\phi_u^* : u \in U\}$, \mathcal{R}

Ensure: Global haplotype matrix $H^* \in \{0, 1, ' -'\}^{K \times L}$, block assignments $\mathbf{b} \in (\mathbb{N} \cup \{\text{NaN}\})^L$

```

1: Initialize:
2:  $U^{\text{phased}} \leftarrow \emptyset$  ▷ Set of phased vertices in  $Q$  (initially empty).
3:  $U^{\text{unphased}} \leftarrow U$  ▷ Set of unphased vertices in  $Q$ . Note: Vertices in  $Q$  include pairs of positions.
4:  $S^{\text{phased}} \leftarrow \emptyset$  ▷ Set of phased variants in  $L$ . Note, this algorithm phases variant by variant
5:  $S^{\text{unphased}} \leftarrow \{1, \dots, L\}$ 
6:  $\text{block\_id} \leftarrow 1$ 
7:
8: Select first node  $u_{\ell_0 \ell_1} \in U^{\text{unphased}}$  in topological order
9:  $H^*[\cdot, \{\ell_0, \ell_1\}] \leftarrow \phi_{u_{\ell_0 \ell_1}}^*$ 
10:  $U^{\text{phased}} \leftarrow \{u_{\ell_0 \ell_1}\}$ ,  $U^{\text{unphased}} \leftarrow U^{\text{unphased}} \setminus \{u_{\ell_0 \ell_1}\}$ 
11:  $S^{\text{phased}} \leftarrow \{\ell_0, \ell_1\}$ ,  $S^{\text{unphased}} \leftarrow S^{\text{unphased}} \setminus \{\ell_0, \ell_1\}$ 
12:  $\mathbf{b}[\{\ell_0, \ell_1\}] \leftarrow \text{block\_id}$ 
13:
14: while  $S^{\text{unphased}} \neq \emptyset$  do
15:    $\mathcal{N} \leftarrow \{u \in U^{\text{unphased}} : \exists v \in U^{\text{phased}}, (v, u) \in E_Q \text{ or } (u, v) \in E_Q\}$  ▷ Neighbor nodes to the phased node set.
16:   if  $\mathcal{N} = \emptyset$  then ▷ There is a disconnected component
17:      $\text{block\_id} \leftarrow \text{block\_id} + 1$ 
18:     Select the next node  $u_{\ell_i \ell_j} \in U^{\text{unphased}}$  in topological order
19:      $H^*[\cdot, \{\ell_i, \ell_j\}] \leftarrow \phi_{u_{\ell_i \ell_j}}^*$ 
20:      $U^{\text{phased}} \leftarrow U^{\text{phased}} \cup \{u_{\ell_i \ell_j}\}$ ,  $U^{\text{unphased}} \leftarrow U^{\text{unphased}} \setminus \{u_{\ell_i \ell_j}\}$ 
21:      $S^{\text{phased}} \leftarrow S^{\text{phased}} \cup \{\ell_i, \ell_j\}$ ,  $S^{\text{unphased}} \leftarrow S^{\text{unphased}} \setminus \{\ell_i, \ell_j\}$ 
22:      $\mathbf{b}[\{\ell_i, \ell_j\}] \leftarrow \text{block\_id}$ 
23:     continue
24:   end if
25:
26:   for each position  $\ell \in S^{\text{unphased}}$  appearing in  $\mathcal{N}$  do
27:      $\text{connectivity}(\ell) \leftarrow |\{u \in \mathcal{N} : \ell \in u\}|$ 
28:   end for
29:    $\ell^* \leftarrow \arg \max_{\ell} \text{connectivity}(\ell)$ 
30:
31:    $\mathbf{h}_{\ell^*} \leftarrow \text{PHASEPOSITION}(\ell^*, S^{\text{phased}}, H^*, \mathcal{N}, \{\phi_u^*\}, \mathcal{R})$ 
32:
33:    $H^*[\cdot, \ell^*] \leftarrow \mathbf{h}_{\ell^*}$ 
34:    $S^{\text{phased}} \leftarrow S^{\text{phased}} \cup \{\ell^*\}$ ,  $S^{\text{unphased}} \leftarrow S^{\text{unphased}} \setminus \{\ell^*\}$ 
35:    $\mathbf{b}[\ell^*] \leftarrow \text{block\_id}$ 
36:
37:   for each  $u \in \mathcal{N}$  where  $\ell^* \in u$  do
38:      $U^{\text{phased}} \leftarrow U^{\text{phased}} \cup \{u\}$ ,  $U^{\text{unphased}} \leftarrow U^{\text{unphased}} \setminus \{u\}$ 
39:   end for
40: end while
41: return  $H^*, \mathbf{b}$ 

```

E.2 Phasing Selected Variant

This algorithm determines the haplotype assignment for a selected position ℓ^* by evaluating candidate phasings based on read evidence and consistency with already-phased positions.

Candidate Generation. A candidate phasing is a haplotype matrix $\mathbf{C} \in \{0, 1\}^{K \times |\mathcal{V}|}$ where \mathcal{V} contains position ℓ^* and a subset of positions from S^{phased} . The size of \mathcal{V} varies by candidate depending on which nodes are used for generation. Candidates are constructed from the potentials on the edges that connects the nodes in the neighbor set \mathcal{N} (unphased nodes adjacent to phased nodes in Q) that contain position ℓ^* to the phased node set and the nodes potentials.

For each node $u_{\ell_i \ell_j} \in \mathcal{N}$ where $\ell^* \in \{\ell_i, \ell_j\}$, we extract phasings $\phi_{\ell_i \ell_j}$ from the node's state space $\Phi_{\ell_i \ell_j}$ that satisfy two conditions: (1) the phasing has non-zero node potential $f(\phi_{\ell_i \ell_j}) > 0$, indicating support from at least one read, and (2) some permutations of the phasing is consistent with the already-assigned haplotypes at any shared positions in $S^{\text{phased}} \cap \{\ell_i, \ell_j\}$. When multiple nodes in \mathcal{N} contain ℓ^* , we combine their phasings to form candidates that maintain consistency across all shared positions under appropriate permutation alignments. Each resulting candidate assigns values to position ℓ^* along with positions from the nodes used in its construction.

Candidate Scoring. Each candidate \mathbf{C} is evaluated using three metrics, which are normalized to $[0, 1]$ within each iteration and combined with weights summing to 1.

Likelihood ($L(\mathbf{C})$): Measures how well candidate \mathbf{C} explains observed reads covering positions in \mathcal{V} . For each read r covering at least one position in \mathcal{V} , we compute the likelihood as defined in Section 3.1, generalized to the positions in \mathcal{V} :

$$L(\mathbf{C}) = \sum_{r \in \mathcal{R}(\mathcal{V})} \log \sum_{k=1}^K \varepsilon^{d(\mathbf{C}^{(k)}, r[\mathcal{V}])} (1 - \varepsilon)^{|\text{cov}(r)| - d(\mathbf{C}^{(k)}, r[\mathcal{V}])},$$

where $\mathbf{C}^{(k)}$ is haplotype k in the candidate, $r[\mathcal{V}]$ are the observed alleles in read r at positions \mathcal{V} , $d(\cdot, \cdot)$ is Hamming distance over covered positions, $|\text{cov}(r)|$ is the number of positions in \mathcal{V} covered by r , and ε is the sequencing error rate.

Minimum Error Correction ($M(\mathbf{C})$): Counts the minimum number of read alleles that must be corrected to achieve consistency:

$$M(\mathbf{C}) = \sum_{r \in \mathcal{R}(\mathcal{V})} \min_{k=1, \dots, K} d(\mathbf{C}^{(k)}, r[\mathcal{V}]).$$

Inference Agreement ($F(\mathbf{C})$): Counts how many nodes in \mathcal{N} have their inferred phasings ϕ_u^* (from Viterbi or FFBS) matched by the candidate under haplotype permutation.

After normalizing each metric to the range $[0, 1]$ by min-max scaling within the current candidate set, the final score is:

$$S(\mathbf{C}) = w_L \cdot \tilde{L}(\mathbf{C}) - w_M \cdot \tilde{M}(\mathbf{C}) + w_F \cdot \tilde{F}(\mathbf{C}),$$

where \tilde{L} , \tilde{M} , \tilde{F} denote normalized scores, weights satisfy $w_L + w_M + w_F = 1$, and default values are $w_L = 1/12$, $w_M = 10/12$, $w_F = 1/12$. The candidate maximizing $S(\mathbf{C})$ is selected, and its column for position ℓ^* is assigned to the global haplotype matrix.

Fallback Strategy. If no valid candidates can be generated due to sparse coverage or lack of connecting nodes, the algorithm uses the inferred phasing $\phi_u^*[\ell^*]$ from any node u containing ℓ^* . This ensures all positions receive assignments while maintaining consistency with the probabilistic inference in regions where read evidence is uninformative.

Algorithm E.2 PHASEPOSITION: Phase Selected Position

Require: Selected position ℓ^* , phased positions S^{phased} , global haplotypes H^* , neighbor nodes \mathcal{N} , inferred phasings $\{\phi_u^*\}$, reads \mathcal{R} , weights (w_L, w_M, w_F)

Ensure: Haplotype column $\mathbf{h}_{\ell^*} \in \{0, 1\}^K$

```

1: Generate Candidates:
2: candidates  $\leftarrow \emptyset$ 
3: for each node  $u \in \mathcal{N}$  where  $\ell^* \in u$  do
4:   for each phasing  $\phi_u$  with  $f(\phi_u) > 0$  do
5:     if  $\exists$  permutation making  $\phi_u$  consistent with  $H^*[S^{\text{phased}}]$  then
6:       Construct candidate  $\mathbf{C}$  from  $\phi_u$  and edge potentials
7:       candidates  $\leftarrow$  candidates  $\cup \{\mathbf{C}\}$ 
8:     end if
9:   end for
10: end for
11:
12: if candidates  $= \emptyset$  then
13:   return  $\phi_u^*[\ell^*]$  for any  $u \in \mathcal{N}$  containing  $\ell^*$ 
14: end if
15:
16: Score Candidates:
17: for each  $\mathbf{C}$  in candidates do
18:   Compute  $L(\mathbf{C}), M(\mathbf{C}), F(\mathbf{C})$ 
19:   Normalize to  $\tilde{L}, \tilde{M}, \tilde{F} \in [0, 1]$ 
20:    $S(\mathbf{C}) \leftarrow w_L \cdot \tilde{L} - w_M \cdot \tilde{M} + w_F \cdot \tilde{F}$ 
21: end for
22:
23: return column for  $\ell^*$  from  $\arg \max_{\mathbf{C}} S(\mathbf{C})$ 

```

F Simulated data

F.1 Polyploid Genomes Simulated from *S. Tuberosum*

Using a reference haplotype from the *S. tuberosum* dataset [35], we simulate full genomes to emulate autopolyploid and allopolyploid configurations. We adapt a version of Haplogenerator from the HaploSim v1.8 software package [30]. Haplogenerator generates random mutations on a reference haplotype using a certain probabilistic model (we choose Poisson) with specific mutation rate parameters for the model. We specify mutation rates (`-s` $[\mu, 0, 0]$) such that μ is the rate of a single nucleotide mutation, and there are no insertions or deletions.

Autopolyploid In autopolyploid genomes, haplotypes are derived from the same species [36]. To generate data for the autopolyploid case, we consider configurations of ploidies 2 (simple diploid, not polyploid), 3, 4, and 6. For each ploidy, k , we generate k haplotypes from the original *S. tuberosum* haplotype, each with mutation rate, μ , where $\mu \in \{0.001, 0.005, 0.01\}$ (each μ is a separate configuration). We do this 20 times per ploidy-mutation rate configuration to generate 20 samples.

Allopolyploid Allopolyploid genomes occur when divergent species merge and their genomes are hybridized [36]. In the allopolyploid case, first we generate two configurations of subgenomes, each set with divergent haplotypes A , B , and C representing the ancestors of each subgenome. These subgenomes are simulated from the original haplotype with mutation rates $\mu_{\text{sub}} \in \{0.0001, 0.0005\}$. Given these subgenome configurations, we simulate further configurations of haplotypes with mutation rates $\mu_{\text{within}} \in \{0.00005, 0.0001\}$ from these diverged subgenome haplotypes. We examine three different allopolyploid structures: a triploid organism with unbalanced subgenome structure (AAB), a tetraploid organism with a balanced structure of two subgenomes (AABB), and a hexaploid organism with a balanced structure of three subgenomes (AABBCC)(Figure F.6).

F.2 Read Simulation

For each simulated polyploid genome configuration, we generated both short-read and long-read sequencing data at multiple coverage depths to evaluate phasing performance across different sequencing technologies and data availability scenarios.

Short-Read Simulation (Illumina) Short paired-end reads were simulated using ART [22] (v2.5.8) with the HiSeq 2500 error profile (`-ss HS25`), which models Illumina sequencing characteristics including position-specific quality scores and systematic errors. We configure ART with the following parameters: read length of 125 bp (`-l 125`), mean fragment size of 350 bp (`-m 350`), standard deviation of 50 bp (`-s 50`), and coverage depths of 3 \times , 5 \times , 10 \times , 20 \times , and 40 \times per haplotype for autopolyploid short read data, and 5 \times , 10 \times , 20 \times , and 40 \times for other configurations. The target coverage was distributed equally across all haplotypes (e.g., for a tetraploid genome at 20 \times total coverage, each haplotype received 5 \times coverage). These parameters represent typical Illumina paired-end sequencing protocols with insert sizes suitable for standard library preparation. The simulated reads maintain consistent quality metrics across all configurations (Figure F.4). In total, we generated 1200 short-read samples for autopolyploid data, and 480 for short-read allopolyploid data (Table F.1).

Long-Read Simulation (Oxford Nanopore) Long reads were simulated using PBSIM3 [31] with the QSHMM-ONT-HQ error model (`-qshmm QSHMM-ONT-HQ.model1`), which accurately replicates Oxford Nanopore Technologies (ONT) high-quality read characteristics including length distribution, error profiles, and base quality scores typical of modern R10.4 chemistry. The simulation used whole-genome strategy (`-strategy wgs`) at coverage depths of 5 \times , 10 \times , 20 \times , and 40 \times per haplotype. The QSHMM-ONT-HQ model produces reads with mean base quality of Q13-14, consistent with contemporary ONT sequencing, and includes realistic error modes dominated by insertion and deletion errors in homopolymer regions. We generated 960 and 480 long-read samples for autopolyploid and allopolyploid data (Table F.1, Figures F.5, F.8).

Read Alignment and Fragment Extraction Short reads were aligned to the reference genome using BWA-MEM (v0.7.17) with default parameters, and long reads were aligned using Minimap2 (v2.24) with the ONT preset (-x map-ont). Alignments were sorted and indexed using SAMtools (v1.15). Then haplotype-informative fragments were extracted from aligned reads using extractHAIRS from the Hap10 [27] suite. For short-read data, we used the default minimum base quality threshold of Q13 (-mbq 13), which is standard for high-quality Illumina data and filters bases with >95% accuracy. For long-read ONT data, we set a more permissive threshold of Q4 (-mbq 4) to account for the characteristically lower per-base quality of ONT sequencing (mean Q13-14). (Tables F.1 and Figures F.2 to F.9.)

Dataset	Ploidy	Mutation Rate	Coverage	# Samples	Total Samples
Autopolyploidy (Short read)	4 (2, 3, 4, 6)	3 (0.001, 0.005, 0.1)	5 (3, 5, 10, 20, 40)	20	1200
Autopolyploidy (Long read)	4 (2, 3, 4, 6)	3 (0.001, 0.005, 0.1)	4 (5, 10, 20, 40)	20	960
Allopolyploidy (Short read)	3 (3: AAB, 4: AABB, 6: AABBC)	4: (0.0001, 0.0005) combine with (0.00005, 0.0001)	4 (5, 10, 20, 40)	10	480
Allopolyploidy (Long read)	3 (3: AAB, 4: AABB, 6: AABBC)	4: (0.0001, 0.0005) combine with (0.00005, 0.0001)	4 (5, 10, 20, 40)	10	480

Table F.1: Datasets Configurations

F.3 Additional Experimental Data Preprocessing Details

Read quality was assessed using FASTQC v0.12.1 and multiqc v1.24.1 [34,15]. Raw reads were subsequently adapter- and quality-trimmed using fastp v0.23.4 with the following quality filtration parameters: --trim_poly_x --length_required 30. Biallelic variants were subsequently filtered for a minimum read depth (FORMAT/DP) of 10, a minimum primary and alternate allele mapping quality of 20 (INFO/MQM and INFO/MQMR, respectively), and homozygous genotypes were manually excluded and using bcftools v1.21 [16]. The accompanying coordinate-sorted BAM files were filtered for a minimum mapping quality (MAPQ) of 20 using samtools v1.20.

F.4 Evaluation Criteria

Generalized vector error rate block types 3 and 4. For blocks of type 4, we approximate the “expected” vector error rate by considering all of the valid bijections at each SNP position besides the first uniformly and compute the expected number of non-fixed points from an arbitrary but fixed permutation considered at the previous position, and sum over positions besides the first. We remark that a valid matching can be viewed as the combination of any permutation of the 0 alleles with any permutation of the 1 alleles; a specific consequence of this is that if there are one or fewer of a certain allele then the permutation of that allele type is over one or fewer elements so we cannot have any moved points. Using a well-known result from algebra, we have that the expected number of fixed points of a permutation of two or more elements is 1, so we get that the expected vector error over an empty block is

$$\sum_{\ell=2}^L (K - \mathbb{I}\{g[\ell] > 1\} - \mathbb{I}\{K - g[\ell] > 1\}), \quad (12)$$

where $\mathbb{I}\{g[\ell] > 1\}$ and $\mathbb{I}\{K - g[\ell] > 1\}$ are the number of haplotypes that we expect *not* to contribute vector errors from the 1 alleles and 0 alleles respectively.

For blocks of type 3, let \tilde{K} , $1 \leq \tilde{K} < K$ be the number of haplotypes phased within the block. We first find the actual vector error by taking the best matching over what has been phased with the ground truth,

where each $\phi_\ell : \{1, \dots, \tilde{K}\} \rightarrow \{1, \dots, K\}$, obviously not surjective. Then, we take the remaining $K - \tilde{K}$ haplotypes left unphased, note the number of each allele type left over (reference and alternate), and compute the expected number of vector errors as we did for type 4 blocks, and report the total block vector error as the sum of the actual and expected contributions.

F.5 Autopolyploidy Data

SNP counts and inter snps distances Here we plot the SNP count information among different ploidies and mutation rates in autopolyploidy data, ranging from almost 500 snps to less than 4000 snps per sample. We also plot the SNP density in the simulated data. Increasing mutation rate decreases inter-SNP gap sizes, while ploidy influences the spacing more weakly. Together, panels (a) and (b) characterize how mutation rate and ploidy shape SNP abundance and genomic distribution in simulated autopolyploid genomes.

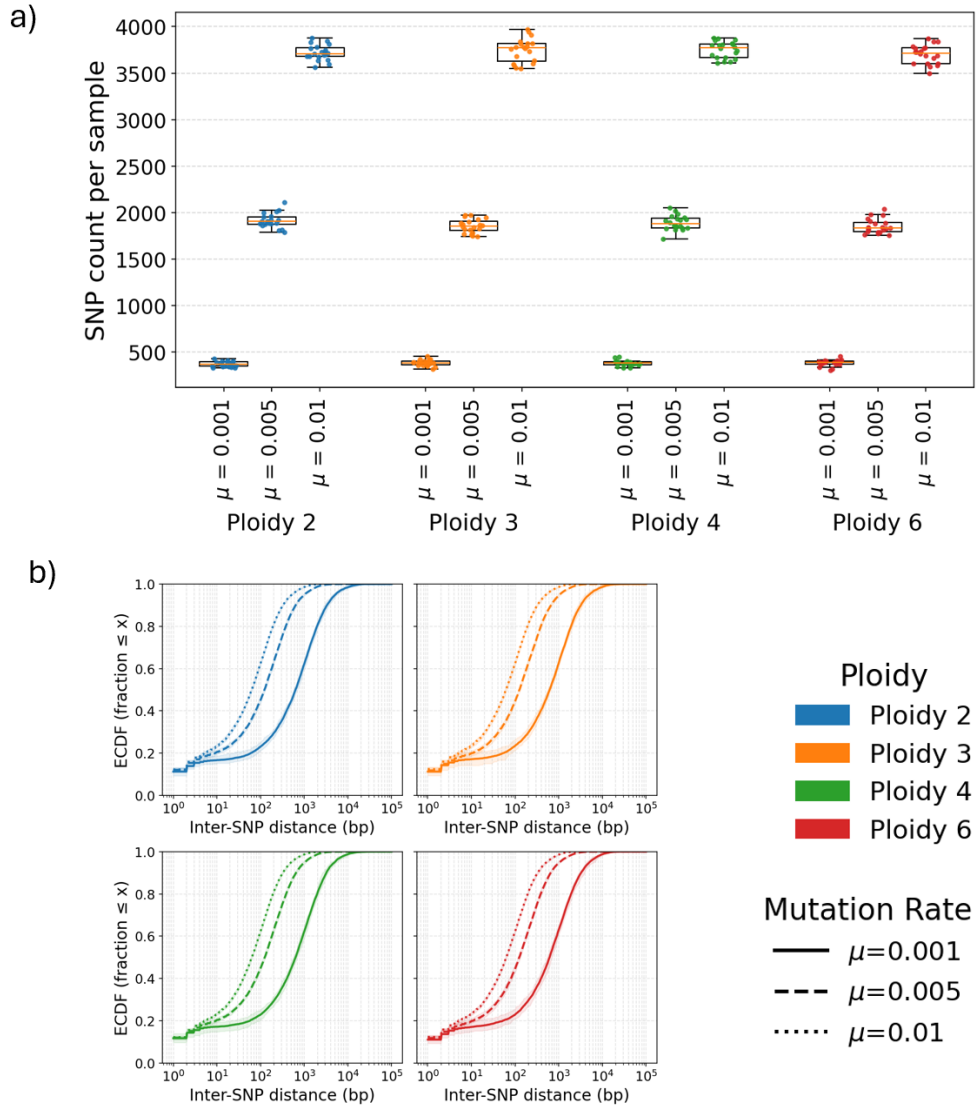


Fig. F.2: **Autopolyploid SNP density and spacing characteristics.** (a) SNP counts per simulated sample across ploidy levels (2, 3, 4, 6) and mutation rates $\mu \in \{0.001, 0.005, 0.01\}$. Boxplots summarize variation across replicates, and points show individual samples, colored by ploidy. Higher mutation rates lead to increased SNP counts, while differences due to ploidy are more modest. (b) Empirical cumulative distribution functions (ECDFs) of inter-SNP distances on a log₁₀ genomic scale. Each curve reflects the mean ECDF across samples for a given ploidy and mutation rate, with shaded bands showing the 10 – 90% range across replicates.

Heatmaps Hamming distance heatmaps showing pairwise distances between simulated haplotypes for autopolyploid configurations (Ploidy 3, 4, 6) across three mutation rates ($\mu \in \{0.001, 0.005, 0.01\}$) for one sample. Values closer to 0 indicate high sequence similarity between haplotypes, while higher values indicate greater divergence.

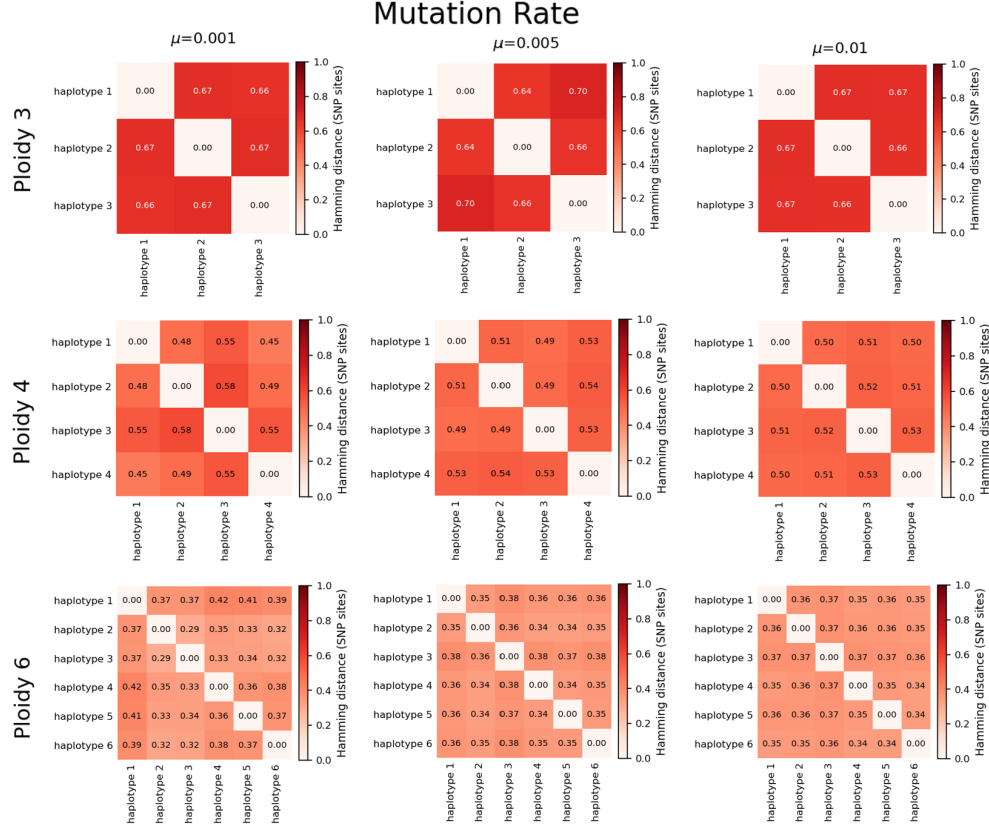


Fig. F.3: **Haplotype pairwise sequence similarity for autopolyploid simulations.** Hamming distance heatmaps showing pairwise distances between simulated haplotypes for autopolyploid configurations (Ploidy 3, 4, 6) across three mutation rates ($\mu \in \{0.001, 0.005, 0.01\}$) for one sample. Values closer to 0 indicate high sequence similarity between haplotypes, while higher values indicate greater divergence.

Short read statistics The plots shows the statistics of the simulated short read sequencing data for autopolyploidy.

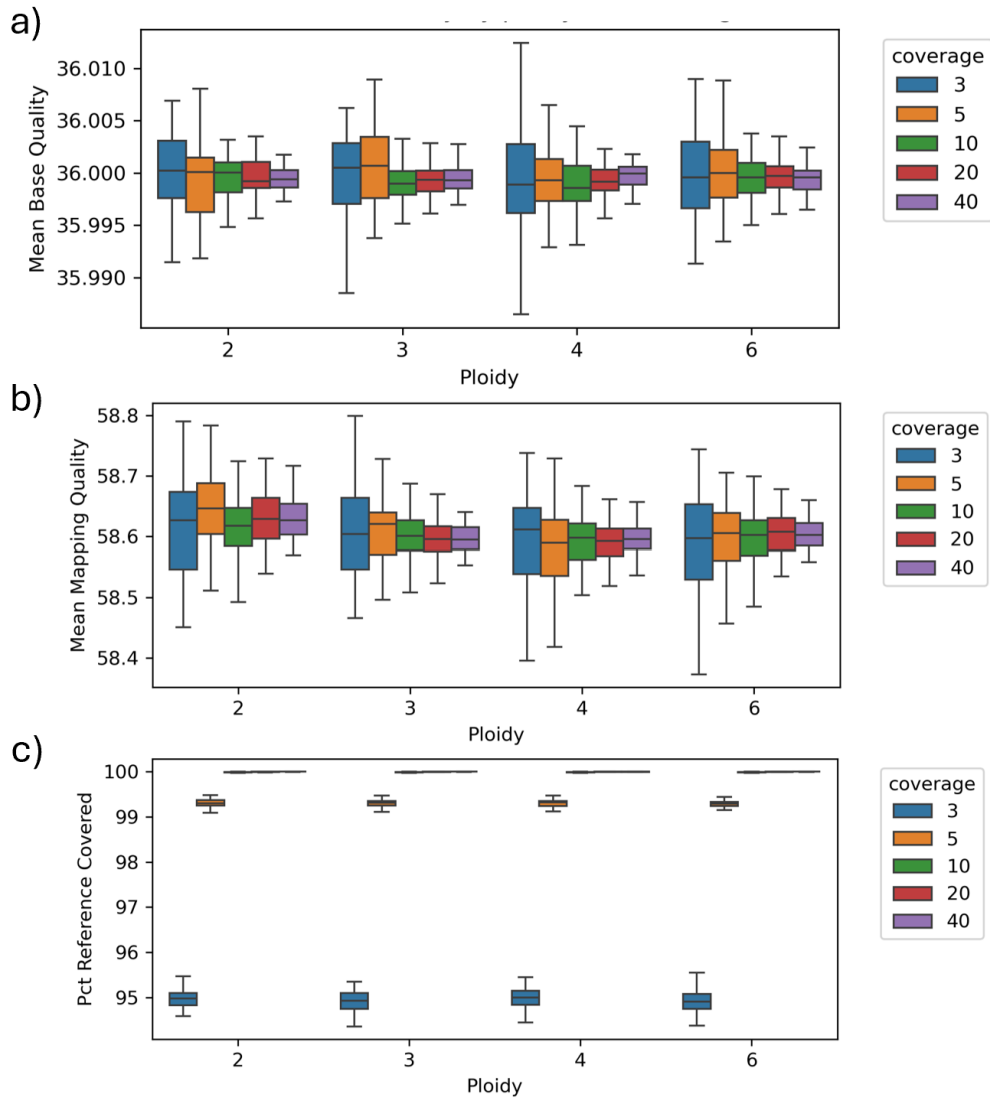


Fig. F.4: **Read and mapping quality characteristics for autopolyploid short-read simulations.** (a) Mean base quality scores, (b) mean mapping quality scores, and (c) percentage of reference genome covered, stratified by ploidy (2, 3, 4, 6) and sequencing coverage (3 \times –40 \times). Quality metrics remain stable across ploidies and coverage levels, confirming consistent read simulation across all configurations.

Long read statistics The plots shows the statistics of the simulated long read sequencing data for autopolyploidy.

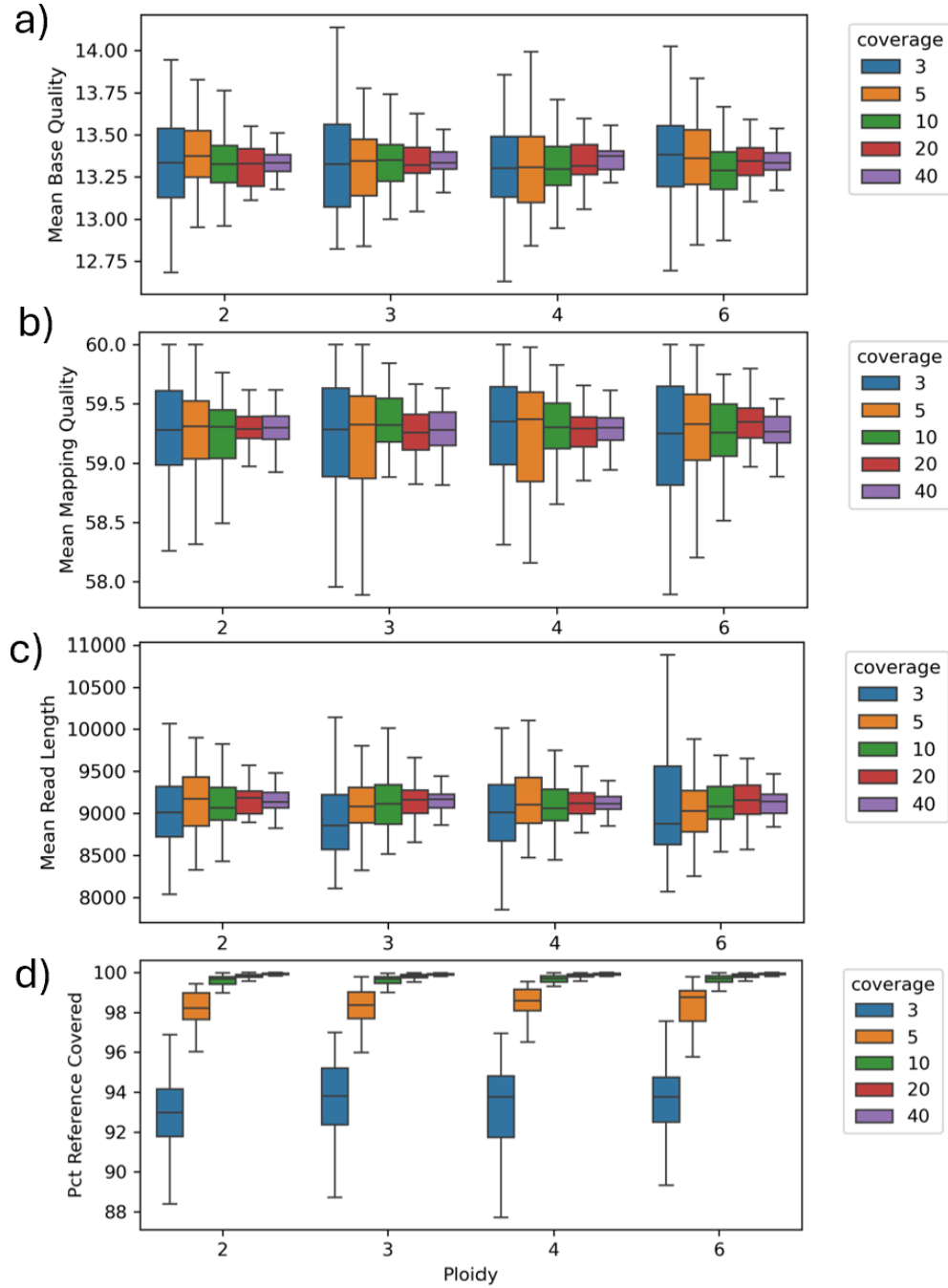


Fig. F.5: **Read metrics for autopolyploid long-read simulations.** (a) Mean base quality, (b) mean mapping quality, (c) mean read length, and (d) percentage of reference covered for autopolyploid samples across ploidy and coverages.

F.6 Allopolyploidy Data

Here we provided detailed information about the Allopolyploidy data:

SNP counts and inter snps distances We first plot the SNP counts and density in the generated dataset.

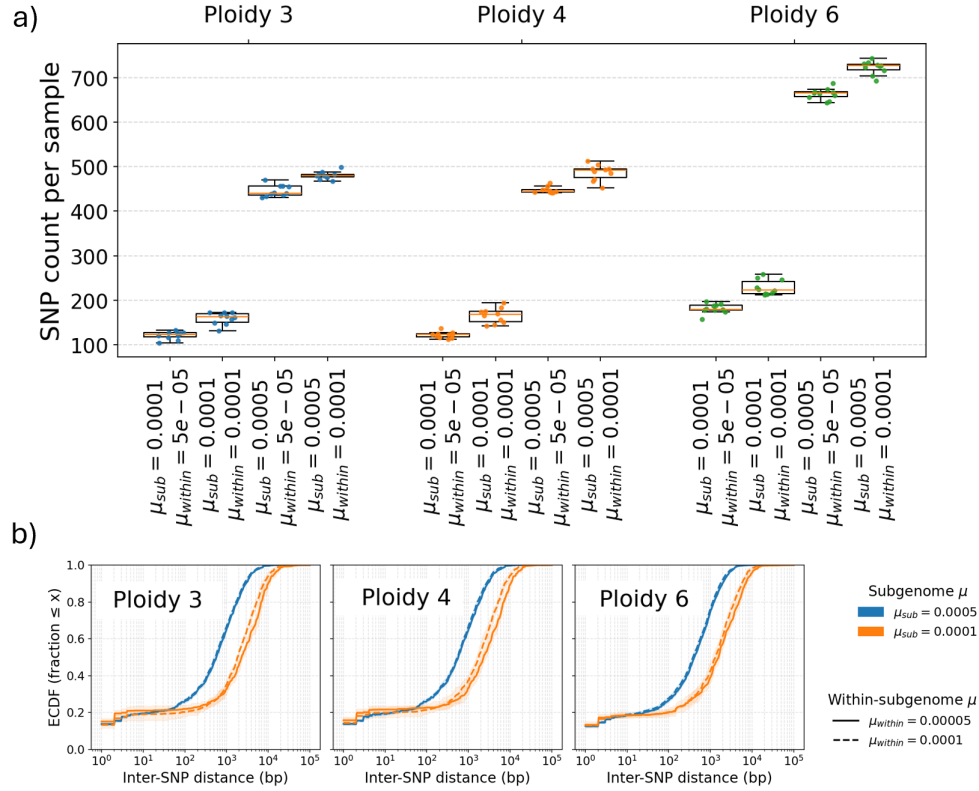


Fig. F.6: **Allopolyploid SNP density and spacing characteristics.** (a) SNP counts per simulated sample across ploidy levels (3: AAB, 4: AABB, 6: AABBCC) and inter-subgenome/within-subgenome mutation rate combinations. (b) Empirical cumulative distribution functions of inter-SNP distances on a \log_{10} genomic scale, showing distinct spacing patterns for subgenome (higher divergence) versus within-subgenome (lower divergence) SNPs.

Heatmaps We plot pairwise Hamming distances between simulated allopolyploid haplotypes across ploidies 3-6 (columns) and mutation rate combinations of subgenome (μ_{sub}) and within-subgenome (μ_{within}) divergence (rows), where darker red indicates greater sequence divergence and block structure reflects subgenome organization.

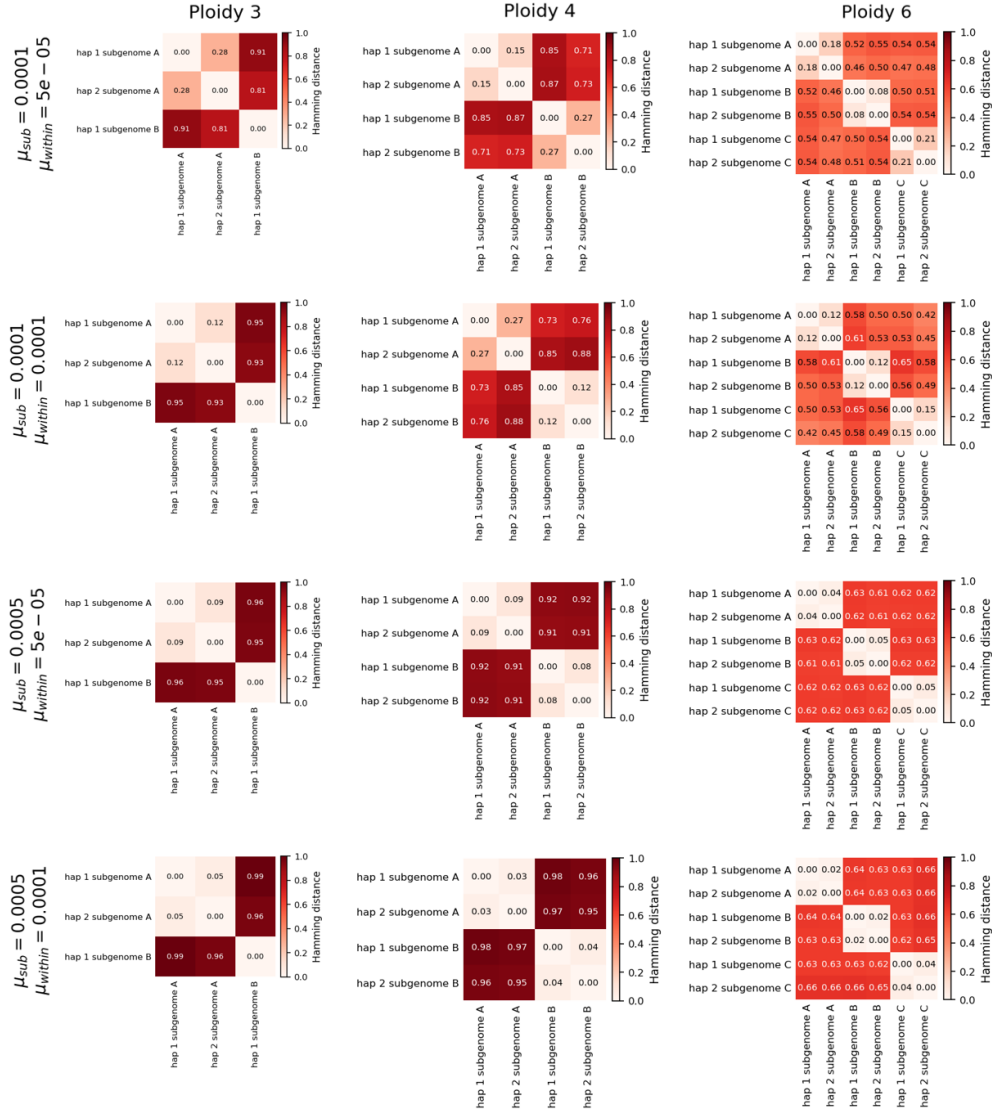


Fig. F.7: **Pairwise haplotype Hamming distances for allopolyploid simulations.** Columns: ploidies 3-6. Rows: inter-subgenome (μ_{sub}) and within-subgenome (μ_{within}) mutation rates. Block structure reflects subgenome organization.

Short read statistics We validated that simulated allopolyploid short-read datasets maintain consistent quality characteristics across all configurations. The plot shows quality metrics remain stable across ploidies and coverage levels, confirming consistent read simulation across all allopolyploid configurations.

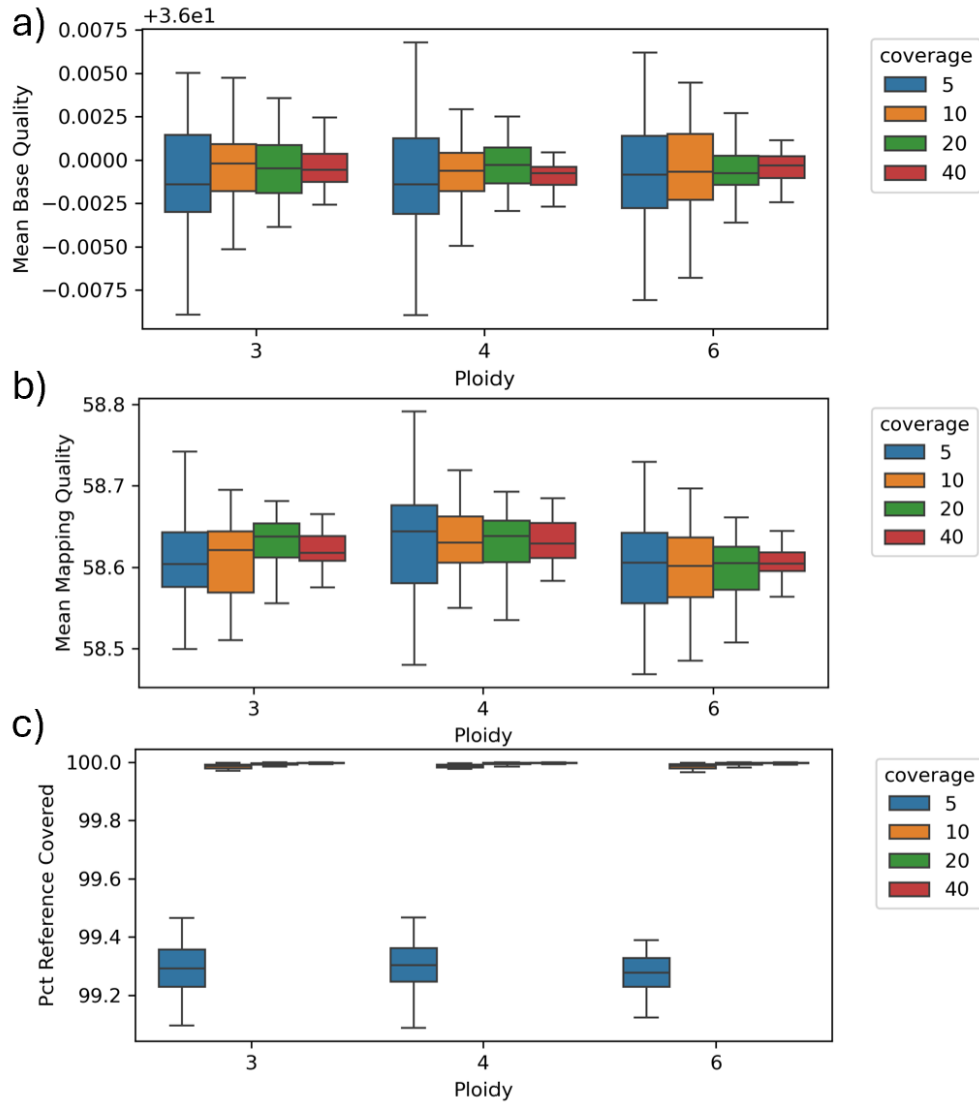


Fig. F.8: **Read and mapping quality metrics for allopolyploid short-read simulations.** (a) Mean base quality scores, (b) mean mapping quality scores, and (c) percentage of reference genome covered by ploidy (3, 4, 6) and sequencing coverage ($5\times$ - $40\times$).

Long read statistics Allopolyploid long-read simulations show stable quality metrics across all ploidies and coverage depths, consistent with modern ONT sequencing characteristics.

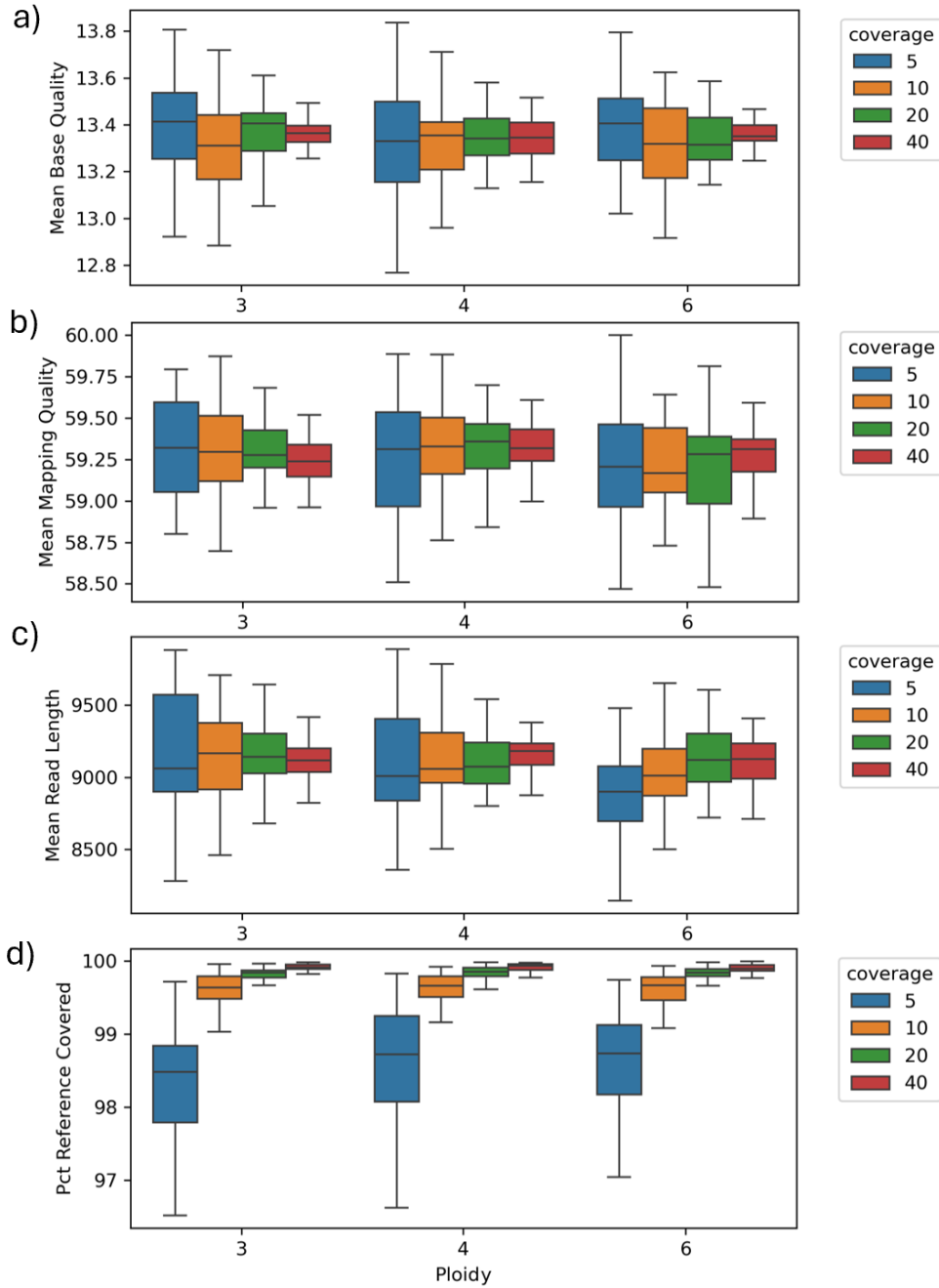


Fig. F.9: **Quality metrics for allopolyploid long-read simulations.** (a) base quality, (b) mapping quality, (c) read length, and (d) reference coverage across ploidies and coverages. Stable metrics confirm realistic ONT simulation.

G Synthetic Results

G.1 Blocks statistics

PHAPCOMPASS-short produces longer average blocks (a) with fewer total blocks (b) than WhatsHap and H-PoPG, particularly at higher ploidies, while maintaining comparable phasing coverage (c). This demonstrates that probabilistic inference maintains phasing continuity where clustering methods fragment due to read assignment ambiguity.

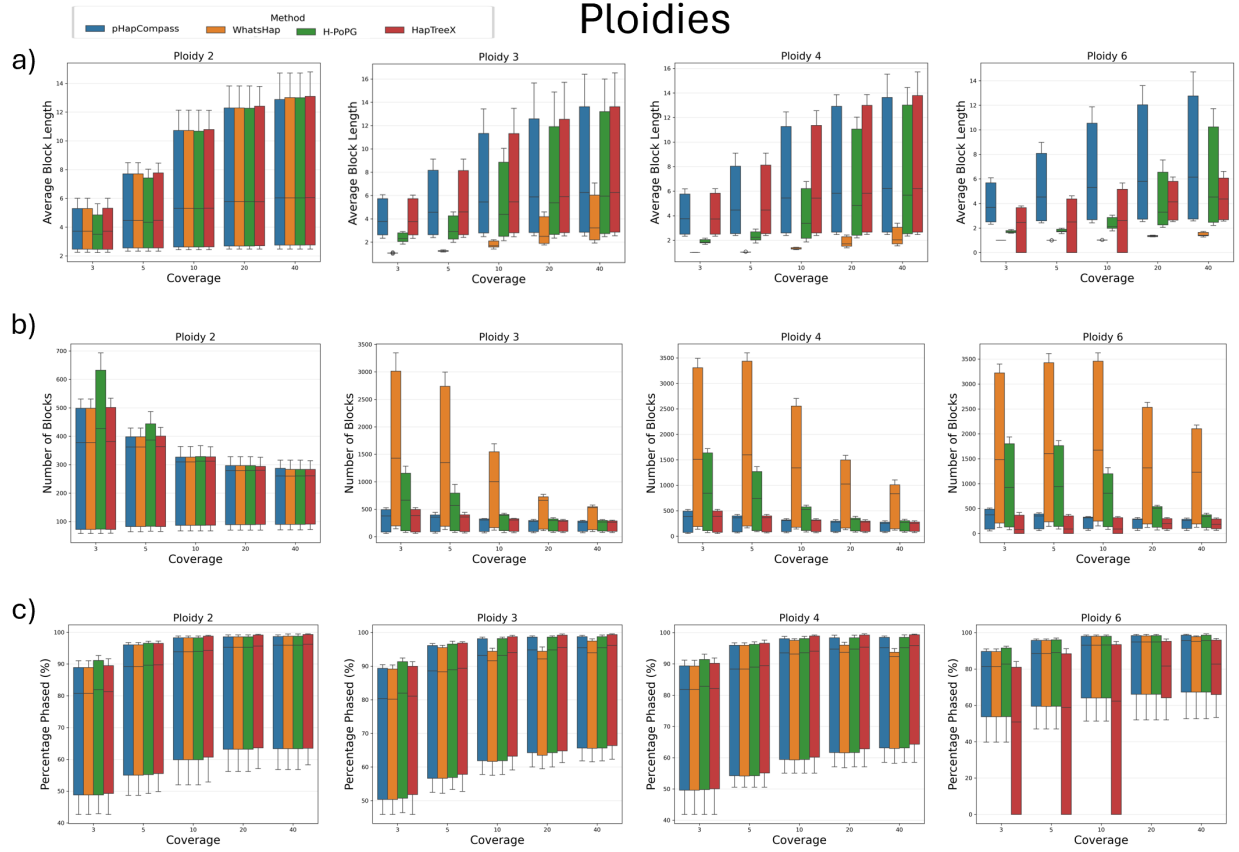


Fig. G.10: **Autopolyploid short-read assembly block statistics.** (a) Average block length in SNPs, (b) total number of phased blocks, and (c) percentage of SNPs phased, by ploidy and coverage for PHAPCOMPASS-short (blue), WhatsHap (orange), H-PoPG (green), and HapTree-X (red).

pHAPCOMPASS-long produces a single-block assemblies at high coverage across all ploidies.

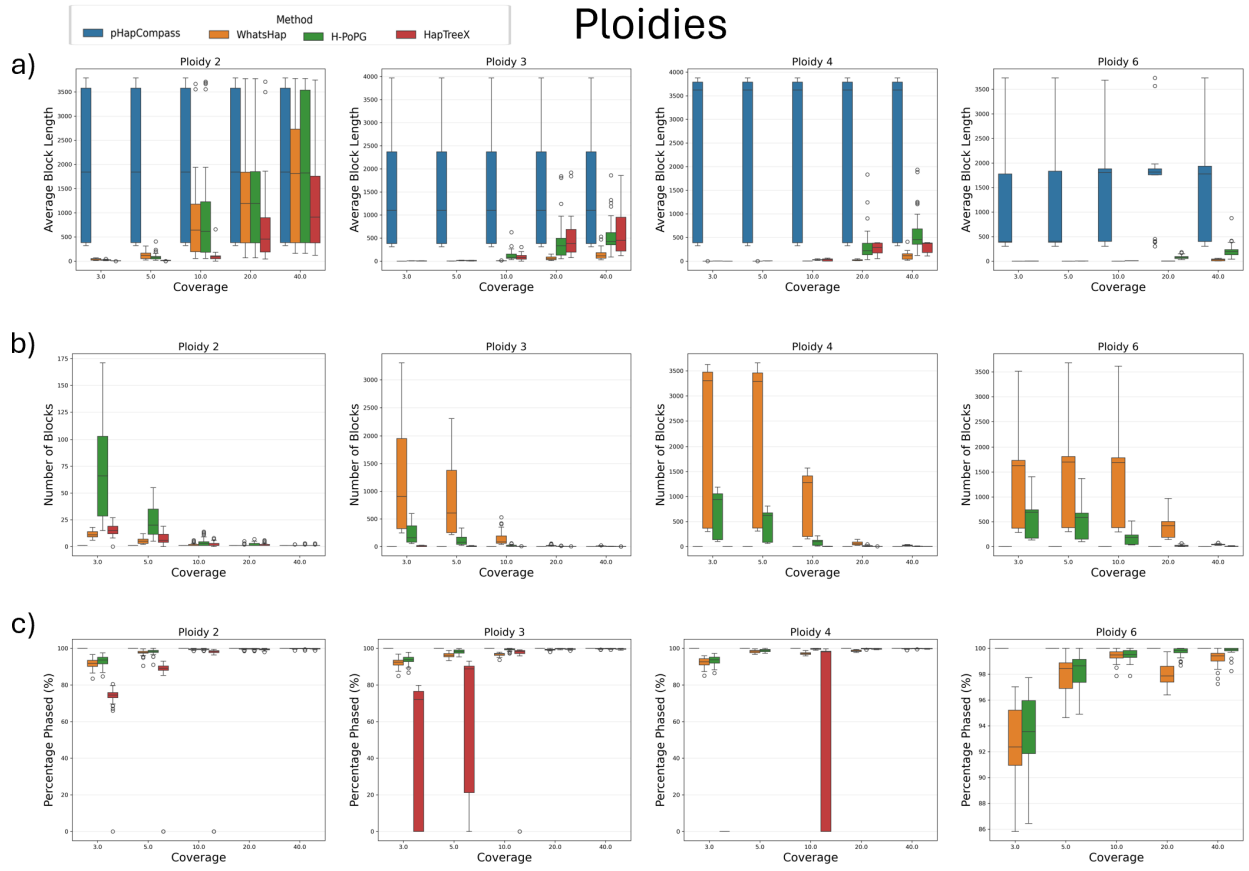


Fig. G.11: **Autopolyploid long-read assembly block statistics.** (a) average block length, (b) number of blocks, (c) percentage phased.

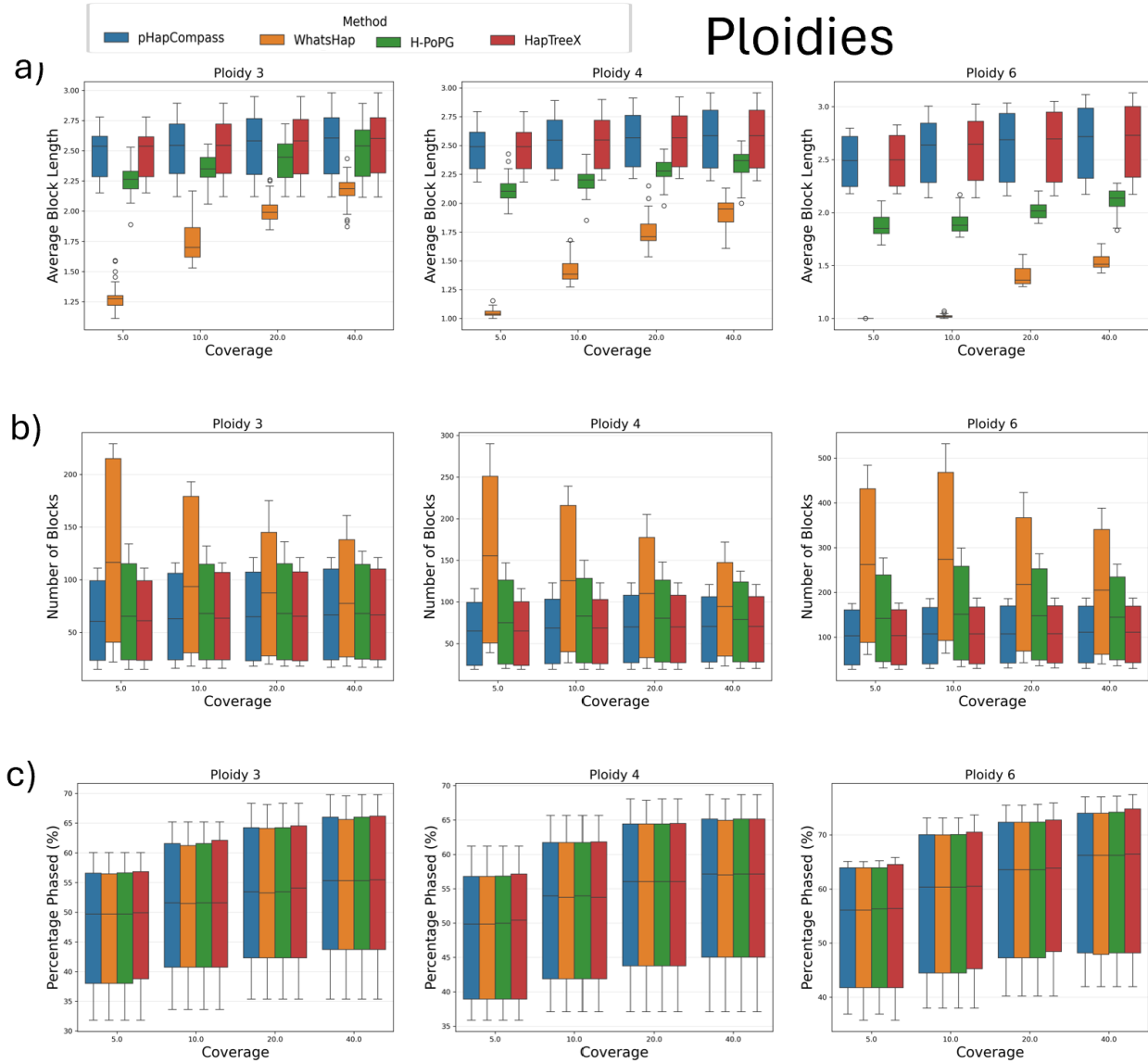


Fig. G.12: **Allopolyploid short-read assembly block statistics.** (a) average block length, (b) number of blocks, (c) percentage phased.

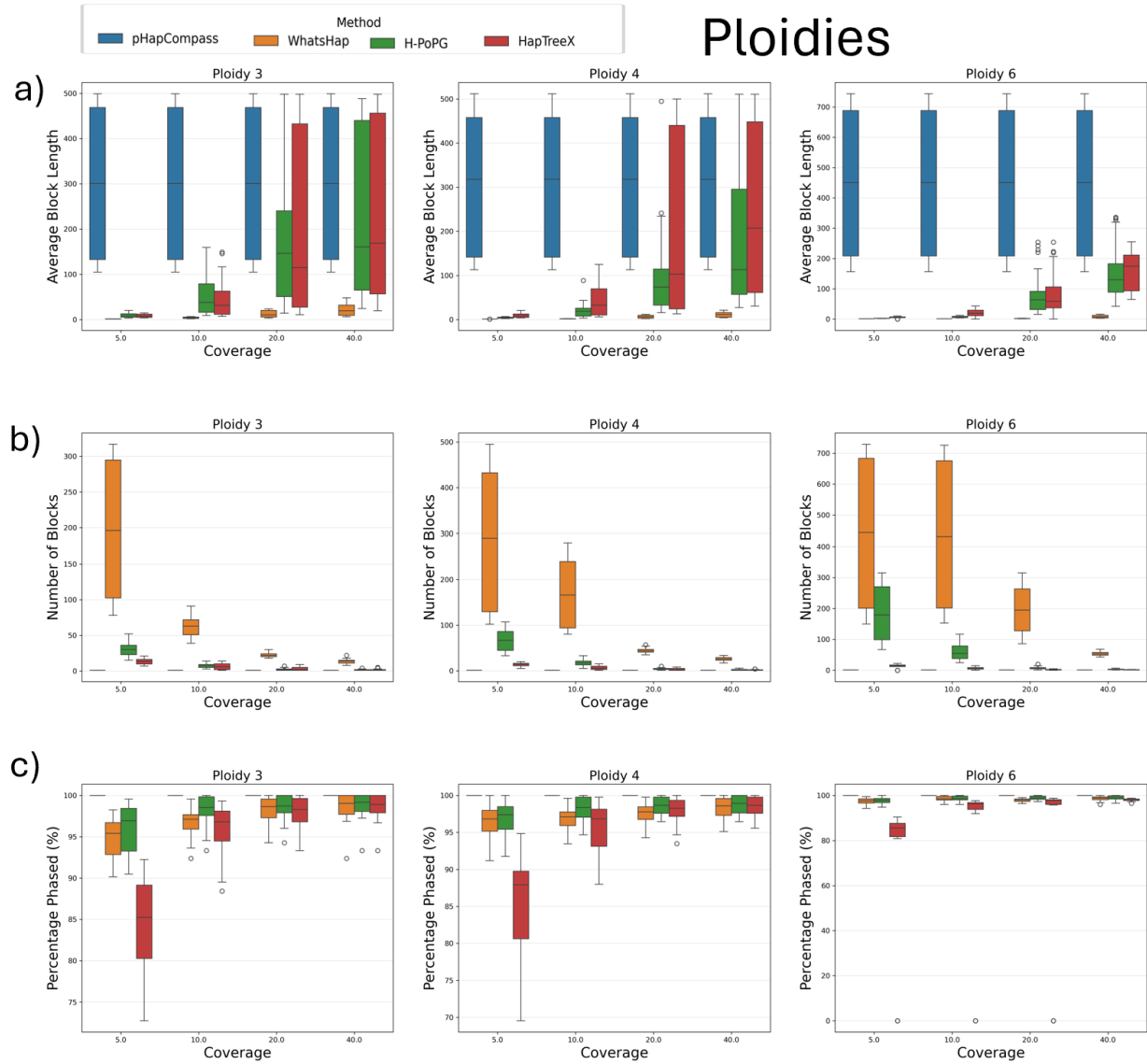


Fig. G.13: **Allopolyploid long-read assembly block statistics.** (a) average block length, (b) number of blocks, (c) percentage phased.

H Experimental Results

Chromosome Number of SNPs	
CM113920.1	110,134
CM113924.1	133,818
CM113928.1	151,179
CM113932.1	125,332
CM113936.1	127,901
CM113940.1	164,036
CM113944.1	104,578
Total	916,978

Table H.2: Chromosome identifiers and SNP counts for experimental octoploid strawberry dataset. All chromosomes were sparsified to maintain minimum 200 bp distance between consecutive SNPs.

Method	Coverage MEC Blocks		
PHAPCOMPASS-short	8×	0.50	126,461
	16×	0.00	84,522
WhatsHap	8×	6.12	691,508
	16×	6.12	754,252
H-PoPG	8×	4.75	485,542
	16×	5.50	527,045

Table H.3: Summarized haplotype assembly performance on experimental octoploid strawberry data aggregated across seven chromosomes. MEC: block-adjusted Minimum Error Correction. Blocks: total number of phased segments.

Method	Chr.	Coverage	# Phased variants	MEC	# Blocks	Block N50 length	Max Lenth
pHAPCOMPASS-short	CM113920.1	8×	2,762	0.00	402	10	43
		16×	2,943	0.00	228	27	91
	CM113924.1	8×	112,835	0.00	20,747	7	87
		16×	123,669	0.00	14,046	17	151
	CM113928.1	8×	126,413	0.00	23,945	7	75
		16×	139,576	0.00	16,222	16	148
	CM113932.1	8×	105,432	0.00	19,919	7	55
		16×	116,145	0.00	13,562	16	142
	CM113936.1	8×	109,092	0.00	19,893	7	84
		16×	119,043	0.00	12,941	18	150
	CM113940.1	8×	139,367	0.50	25,454	7	78
		16×	152,564	0.00	16,898	17	161
	CM113944.1	8×	88,978	0.00	16,101	8	54
		16×	96,863	0.00	10,625	18	190
WhatsHap	CM113920.1	8×	2,784	0.88	2,784	1	1
		16×	2,951	0.88	2,951	1	1
	CM113924.1	8×	113,950	0.88	113,930	1	2
		16×	124,324	0.88	124,247	1	2
	CM113928.1	8×	127,760	0.88	127,732	1	2
		16×	140,337	0.88	140,238	1	2
	CM113932.1	8×	106,464	0.88	106,415	1	2
		16×	116,764	0.88	116,672	1	2
	CM113936.1	8×	110,139	0.88	110,110	1	2
		16×	119,619	0.88	119,541	1	2
	CM113940.1	8×	140,796	0.88	140,764	1	2
		16×	153,368	0.88	153,283	1	2
	CM113944.1	8×	89,796	0.88	89,773	1	2
		16×	97,374	0.88	97,320	1	2
H-PoPG	CM113920.1	8×	2,793	0.50	1,898	2	11
		16×	2,958	0.88	2,093	1	10
	CM113924.1	8×	114,153	0.00	79,366	2	23
		16×	124,283	0.00	86,687	1	33
	CM113928.1	8×	127,980	1.88	89,697	2	28
		16×	140,281	0.50	97,730	1	29
	CM113932.1	8×	106,675	0.50	73,732	2	18
		16×	116,646	0.88	80,839	1	26
	CM113936.1	8×	110,279	1.88	76,238	2	30
		16×	119,582	0.88	83,846	1	38
	CM113940.1	8×	141,087	0.00	100,058	1	18
		16×	153,300	0.50	107,576	1	40
	CM113944.1	8×	89,943	0.00	64,553	1	16
		16×	97,310	1.88	68,274	1	23

Table H.4: Detailed per-chromosome haplotype assembly results for all methods and coverage levels.

I Run time analysis

Runtime measurements were collected on two computing environments: (1) Intel Xeon Gold 6230 @ 2.10GHz, 8GB RAM, Ubuntu 22.04 for PHAPCOMPASS-short, WhatsHap, H-PoPG, and most of the PHAPCOMPASS-long experiments, and (2) Intel Xeon Gold 6242 @ 2.80GHz, 376GB RAM, Ubuntu 24.04 for remaining PHAPCOMPASS-long experiments. HapTree-X was executed on a separate workstation. Due to heterogeneous hardware, absolute runtime comparisons across methods are approximate; we focus on relative scaling within each method.

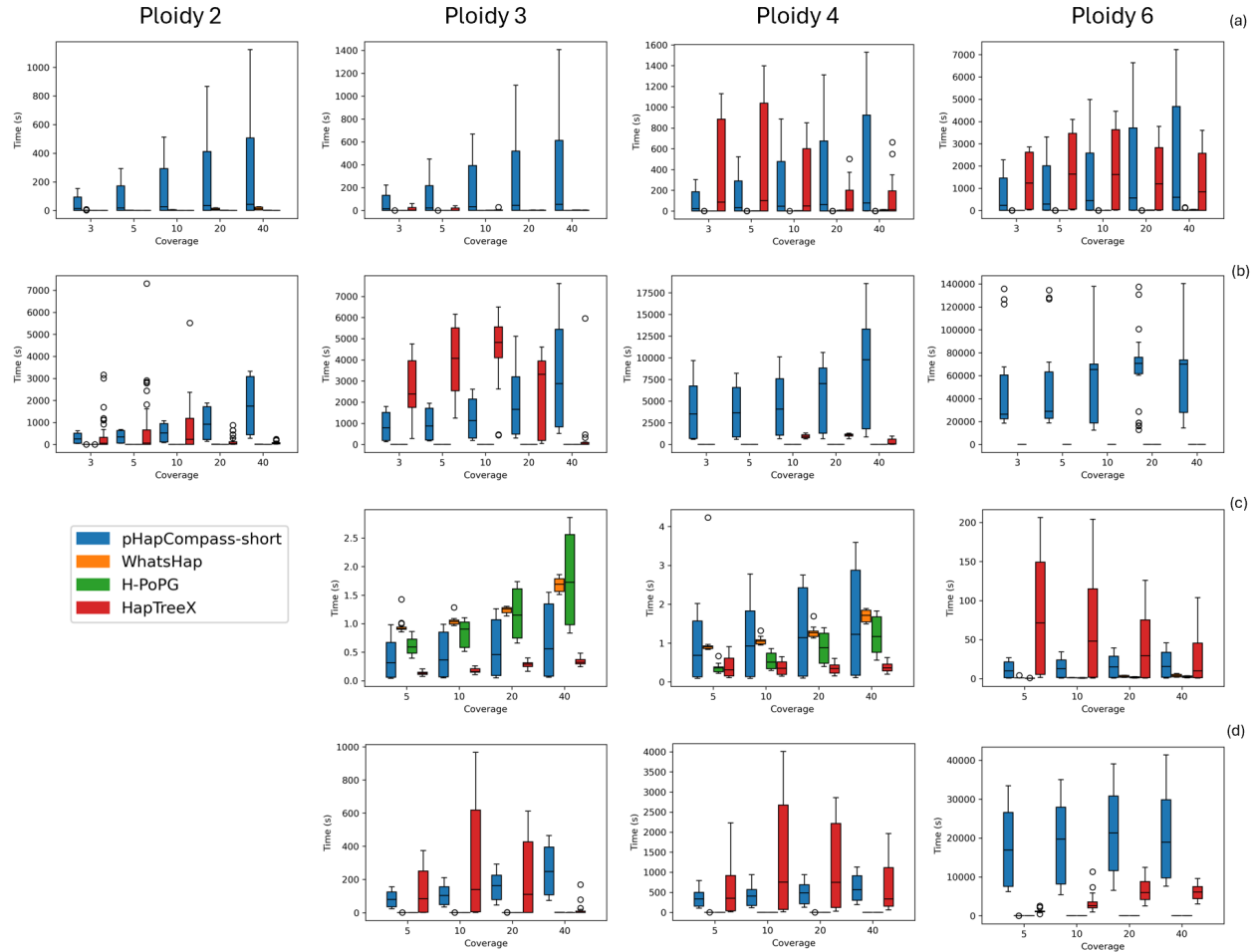


Fig.I.14: **Runtime analysis (seconds)**. The methods are PHAPCOMPASS (blue), WhatsHap (orange), H-PoPG (green), and HapTree-X (red) across ploidy and coverages for (a) autopolyploid short reads, (b) autopolyploid long reads, (c) allopolyploid short reads, and (d) allopolyploid long reads. Measurements collected on heterogeneous hardware; values indicate relative scaling patterns.